Signatures for a Cosmic Flux
of Magnetic Monopoles

Stuart D. Wick[1], Thomas W. Kephart[1], Thomas J. Weiler[1]
and Peter L. Biermann[2]

[1] *Department of Physics & Astronomy, Vanderbilt University,*

Nashville, TN 37235

[2] *Max Planck Institute for Radioastronomy,*

D-53010 Bonn, Germany

Any early Universe phase transition occurring after inflation has the potential to populate the Universe with relic magnetic monopoles. Observations of galactic magnetic fields, as well as observations matched with models for extragalactic magnetic fields, lead to the conclusion that monopoles of mass $\lesssim 10^{15}$ GeV are accelerated in these fields to relativistic velocities. We explore the possible signatures of a cosmic flux of relativistic monopoles impinging on the earth. The electromagnetically-induced signatures of monopoles are reliable. The hadronically-induced signatures are highly model-dependent. Among our findings are (i) the electromagnetic energy losses of monopoles continuously initiate a protracted shower of small intensity; (ii) monopoles may traverse the earth's diameter, making them a probe of the earth's interior structure; (iii) in addition to the direct monopole Cherenkov signal presently employed, a very attractive search strategy for monopoles is detection of their coherent radio-Cherenkov signal produced by the charge-excess in the e^+–e^- shower — in fact, Cherenkov-detectors have the potential to discover a monopole flux (or limit it) several orders of magnitude below the theoretical Parker limit of $10^{-15}/\mathrm{cm}^2/\mathrm{s}/\mathrm{sr}$; (iv) it is conceivable (but not compelling) that bound states of colored monopoles may be the primary particles initiating the air showers observed above the GZK cutoff.

I. INTRODUCTION

Any breaking of a semisimple gauge symmetry which occurs after inflation and which will leave unbroken a $U(1)$ symmetry group may produce an observable abundance of magnetic monopoles. The initial monopole number density can be estimated from the type and temperature of the symmetry breaking phase transition [1]. From this, one easily derives the present day flux of monopoles [2]. The monopole mass is expected to be $\sim \alpha^{-1}$ times the scale Λ_{SB} of the symmetry breaking. It is noteworthy that the inferred strength and coherence size of existing extragalactic

magnetic fields suggest that any monopole with a mass near or less than 10^{14} GeV would have been accelerated in magnetic fields to relativisitic velocities. On striking matter, such as the earth's atmosphere, these relativistic monopoles will generate a particle cascade. It is the purpose of this paper to calculate the shower signatures of relativistic magnetic monopoles. An extensive collection of monopole references covering theoretical investigations and experimental searches prior to 1998 can be found in [3].

The electromagnetic interaction cross–section for relativistic monopoles is fairly well understood, but the hadronic cross–section is not. We calculate in some detail the reliable signatures resulting from the electromagnetic monopole–matter interaction. For the hadronic interactions of the monopole, we investigate various possibilities, and we present qualitative arguments for the resulting signatures.

On theoretical grounds, the flux of monopoles that do not catalyze baryon decay is limited only by Parker's upper bound $F_{\rm P} \sim 10^{-15}/{\rm cm}^2/{\rm s}/{\rm sr}$ [4]. We do not consider monopoles which do catalyze baryon decay, as the flux limits on these render them not observable. The Parker bound results from requiring that monopoles not short–circuit our Galactic magnetic fields faster than the Galactic dynamo can regenerate them. The Parker bound is several orders of magnitude above the observed highest–energy cosmic ray flux. Thus, existing cosmic ray detectors can meaningfully search for a monopole flux, and proposed vast–area cosmic ray detectors may improve the search sensitivity by many orders of magnitude.

Because of the small inelasticity of monopole interactions, the monopole primary will continuously induce an air–shower. This is in contrast to nucleon and photon primaries which transfer nearly all of their energy in the shower initiation. Thus we expect the monopole shower to be readily distinguished from non–monopole initiated showers. However, we also investigate the possibility that the hadronic interaction of the monopole is sufficiently strong to produce air–showers with dE/dx comparable to that from nuclear primaries, in which case existing data would already imply a meaningful limit on the monopole flux. One may even speculate that monopoles with a large dE/dx have been observed, as the primaries producing the enigmatic showers above the GZK cutoff at $\sim 5 \times 10^{19}$ eV [5,6].

The outline of this paper is as follows: In section (II) we discuss the limits on the monopole mass and number density. We discuss the variety of monopoles resulting from possible symmetry breakings, and examine their natural kinetic energies resulting from acceleration in large-scale cosmic magnetic fields. In section (III) expressions for the energy loss of relativistic monopoles are presented. The electromagnetic processes of ionization, electron–pair production, bremsstrahlung, and the photonuclear interaction provide the most reliable expressions. The hadronic energy loss is also considered. In section (IV) we discuss signatures of relativistic monopoles arising from their electromagnetic energy loss processes. We develop a model for the electromagnetic particle shower induced by relativistic monopoles. Cherenkov signatures are also examined, including the coherent radio-Cherenkov signal resulting from the shower charge excess. We mention the possible detection of the coherent Cherenkov signal in km^3 ice experiments. It is shown that for certain masses Earth tomography with monopoles is practicable. The monopole's electromagnetic dE/dx in air appears to be too low to allow their detection via air fluorescence. However, we argue that some speculative models may allow the geometric size of "baryonic–monopoles" to grow as a result of interactions, with the concomitant increase in their strong cross-section leading to significant air fluorescence. This possibility is explored in section (V) with a simple model for the growing strong cross–section. Finally, in section (VI) we give concluding remarks.

II. MONOPOLES AND MAGNETIC FIELDS

A. Monopole Mass and Number Density

As first shown by 't Hooft and Polyakov [7], the dynamical content and stability of magnetic monopoles in particle physics models is regulated by the patterns of symmetry breaking in these models. A classification is given in [8] based on homotopy theory. For illustration, we consider the simplest case of a semisimple gauge group G (i.e., G has no $U(1)$ factors) that breaks to a subgroup G' that is nonsemisimple (i.e., has at least one $U(1)$ factor which is part of a linear combination making up $U_{EM}(1)$). At the symmetry-breaking temperature $T_c \sim \langle \phi \rangle$ at which the order parameter $\langle \phi \rangle$ turns on, monopoles of mass $M \sim T_c/\alpha$ appear, where α is the fine structure constant at scale T_c. The order parameter can be the VEV of some scalar field or some bi-fermionic condensate that breaks the symmetry. We assume that the value of $\langle \phi \rangle$ is at or above the electroweak (EW) scale ~ 250 GeV so as to avoid violations of Standard Model (SM) physics. This assumption then bounds the monopole mass for our consideration to be $\stackrel{>}{\sim} 40$ TeV. We note that a similar lower mass bound results from (boldly) treating a classical monopole as a virtual quantum in radiative corrections to the SM [9].

The number density and therefore the flux of monopoles emerging from a phase transition are determined by the Kibble mechanism [1]. At the time of the phase transition, roughly one monopole or antimonopole is produced per correlated volume. The resulting monopole number density today is

$$n_M \sim 10^{-19} \, (T_c/10^{11} \mathrm{GeV})^3 (l_H/\xi_c)^3 \, \mathrm{cm}^{-3}, \tag{2.1}$$

where ξ_c is the phase transition correlation length, bounded from above by the horizon size l_H at the time when the system relaxes to the true broken–symmetry vacuum. In a second order or weakly first order phase transition, the correlation length is comparable to the horizon size. In a strongly first order transition, the correlation length is considerably smaller than the horizon size. In section (II C) we will show that free monopoles with $M \stackrel{<}{\sim} 10^{15}$ GeV are accelerated to relativistic energies by the cosmic magnetic fields [10]. From Eq.(2.1) then, the general expression for the relativistic monopole flux may be written [6]

$$F_M = c \, n_M/4\pi \sim 2 \times 10^{-4} \left(\frac{M}{10^{15} \mathrm{GeV}} \right)^3 \left(\frac{l_H}{\xi_c} \right)^3 \, \mathrm{cm}^{-2} \, \mathrm{sec}^{-1} \, \mathrm{sr}^{-1} \,. \tag{2.2}$$

Phenomenologically, the monopole flux is constrained by cosmology and by astrophysics. Cosmology requires that the monopole energy density Ω_M not be so large as to add observable curvature to the Universe. From eq. (2.1) comes an expression for the monopole mass density today relative to the closure value

$$\Omega_M \sim 0.1 \, (M/10^{13} \mathrm{GeV})^4 (l_H/\xi_c)^3. \tag{2.3}$$

Monopoles less massive than $\sim 10^{13} (\xi_c/l_H)^{3/4}$ GeV do not over-curve the Universe. Astrophysics requires the monopole flux to respect the Parker bound such that the magnetic field of our galaxy is sustained. Requiring that the Kibble flux in eq. (2.2) be less than the Parker limit $F_P \equiv 10^{-15}/\mathrm{cm}^2/\mathrm{sec}/\mathrm{sr}$, one derives a combined mass bound [6]

$$M \stackrel{<}{\sim} 10^{11} (\xi_c/l_H) \, \mathrm{GeV} \,. \tag{2.4}$$

This constraint is stronger than the curvature constraint by about two orders of magnitude for phase transitions without excessive latent heat.

3

The energy–density constraint for relativistic monopoles is of course stronger than that for non–relativistic monopoles of the same mass. From eqs. (2.3) and (2.2) we may write for the *relativistic* monopole closure density [6]

$$\Omega_{RM} \sim \left(\frac{\langle E_M \rangle}{m_{\mathrm{Pl}}} \right) \left(\frac{F_M}{F_P} \right) , \tag{2.5}$$

where $m_{\mathrm{Pl}} = 1.2 \times 10^{19}$ GeV is the Plank mass. This shows that a Kibble monopole flux respecting the Parker limit cannot over-curve the Universe regardless of the nature of the monopole–creating phase transition (parameterized by ξ_c/l_H), as long as $\langle E_M \rangle \stackrel{<}{\sim} m_{\mathrm{Pl}}$.

Minimal $SU(5)$ breaking gives monopoles of mass $\sim 10^{17}$ GeV. However, within field theory there exist many possibilities to produce monopoles with mass below this scale. For example, there are other chiral $SU(N)$ [11] and chiral $O(N)$ models [12,13] with lighter monopoles. There are also relatively light monopoles ($M \sim 10^8$ GeV) in the phenomenologically interesting $SU(15)$ model [14]. Recently, a new field theoretic possibility has emerged based on conformal field theory (CFT). Although originally conceived in the context of type IIB strings and M-theory compactifications on higher–dimensional anti-de Sitter space [15], the rules for constructing the four-dimensional CFTs can be considered independently of any higher dimensional origins. These theories are naturally $N = 4$ supersymmetric, but depending on the compactification, can have reduced $N = 0$ or 1 supersymmetry and have sensible phenomenology with a product of $SU(N_i)$ gauge groups. Three-family non-supersymmetric models have been constructed with GUT scale as low as a few TeV [16]. These models have light monopoles ~ 100 TeV. Some of these models unify $U_{EM}(1)$ and $SU_C(3)$ [17], while others do not. Thus, monopoles in these models may or may not have hadronic interactions.

In yet another alternative, extra dimensions *a la* Kaluza-Klein [18,19] decrease M_{GUT} if these extra dimensions are not too tightly compactified. For example, with the introduction of two extra dimensions of millimeter size, the GUT scale is lowered to about 100 TeV due to the dramatic change from logarithmic to power law running in the RG-improved running coupling constant. This low–scale unification in turn may lead to magnetic monopoles of mass $\sim 10^4$ TeV. A potential concern for monopoles in higher–dimensional theories is topological instability, i.e., monopoles in greater than four dimensions may unwind. However, monopoles made of SM fields confined to our three–dimensional brane would remain stable. In fact, there are even richer possibilities for monopoles in higher–dimensional theories. New defect solutions may exist in the larger dimensions, stabilized by topology. The intersection of these new solutions on the SM brane could then be monopoles, stabilized by the usual 3D topological argument.

A relatively low GUT scale seems to be necessary to allow light–mass monopoles. A low GUT scale will typically also enable fast proton decay, in violation of experimental lifetime bounds. However, exceptions abound. The $SU(15)$ model has no direct gauge induced proton decay. Proton decay in the MSSM Pati-Salam Model [11] is only induced through the hidden sector. Some of the 4D models listed above have accidental symmetries (continuous or discrete) which stabilize the proton, and the higher dimensional models have additional stabilizing possibilities.

To summarize this section, there are theoretical possibilities for producing monopoles with mass $\stackrel{<}{\sim} 10^{15}$ GeV, while avoiding proton decay. In addition to their electromagnetic properties, these monopoles may have a strong interaction cross–section. In the context of the Kibble mechanism for monopole production, observational bounds on the Universe's curvature constrain the monopole mass to less than 10^{13} GeV. More constraining is a comparison of the Kibble flux to the Parker limit which constrains the monopole mass to less than 10^{11} GeV.

We note that in higher dimensional cosmologies the Kibble flux given in eq. (2.2) may be altered. If the Kibble flux

estimate is changed, then the straightforward Parker upper limit $F_M \leq 10^{-15}/\text{cm}^2/\text{sec}/\text{sr}$ becomes the only reliable bound on the monopole flux. Thus, in the spirit of generality, we will let M be a free parameter and use the Kibble mechanism as a rough guide to F_M. We will, of course, require that F_M obey the Parker limit. We also will assume that proton decay is avoided in a way that does not restrict the parameter M.

B. Monopole Structure

The fact that monopoles are topological defects endows them with a non-trivial internal structure. Monopoles are classified [1] by their topological winding in the group manifold. This topological classification is coarse for GUT monopoles, which require further classification according to their charges. Monopole charges are dual to the SM charges. For example, in a dual theory magnetic charge and chromomagnetic (or color–magnetic) charge replace electric charge and chromoelectric (or color–electric) charge.

Fundamental monopoles can bind to form composite monopoles. For example, in an $SU(5)$ GUT the fundamental minimally-charged monopoles are six-fold degenerate. For an appropriate Higgs potential there are four other types of stable bound states formed from the colored fundamental monopoles [20]. Remarkably, the spectrum of bound–state monopoles corresponds almost exactly to the particle spectrum of a standard model family, which has led to an attempt to construct a "dual standard model" out of monopoles [21].

We adopt the nomenclature "q–monopoles" for those monopoles with color–magnetic charge, and "l–monopoles" for those with only the ordinary $U_{EM}(1)$ magnetic charge. The possible confinement of q-monopoles via the formation of Z_3 color–magnetic "strings" has been considered recently [22]. If such a confinement mechanism is realized, one expected result would be the formation of color–singlet "baryonic–monopoles." Thus we are led to consider the phenomenology of two broad classes of monopoles, the l-monopoles with $U(1)$ magnetic charge, and the baryonic-monopoles with hadronic interactions in addition to electromagnetic interactions.

The baryonic–monopole structure is quite different from that of an l–monopole, and as such we expect it to have a very different cross–section and cosmic ray shower profile. The internal dynamics of a baryonic-monopole would approximate that of an ordinary baryon in the QCD string model, but with q–monopoles replacing quarks at the ends of strings. In particular, the string tensions of the chromomagnetic and chromoelectric strings are both of order Λ_{QCD}. However, the energetics of string-breaking for the two cases are very different. The chromoelectric string of standard QCD will stretch until energetics favors breaking and the production of a quark-antiquark pair. The chromomagnetic string internal to the baryonic-monopole may stretch until energetics favors breaking and the production of a monopole-antimonopole pair. From the large mass of the monopole-antimonopole pair, we infer that an enormous amount of string-stretching without breaking is possible for a baryonic-monopole. In sec. (V) we discuss the viability of baryonic–monopoles as candidate primaries for the super–GZK airshowers.

C. Monopole Acceleration

The kinetic energy imparted to a magnetic monopole on traversing a magnetic field along a particular path is [6]

$$E_K = g \int_{\text{path}} \vec{B} \cdot \vec{dl} \sim g\,B\,\xi\,\sqrt{n} \tag{2.6}$$

where

$$g = e/2\alpha = 3.3 \times 10^{-8} \text{ esu } (\text{or } 3.3 \times 10^{-8} \text{dynes/G}) \tag{2.7}$$

is the magnetic charge according to the Dirac quantization condition, B is the magnetic field strength, ξ specifies the field's coherence length, and $\sqrt{n}$ is a factor to approximate the random–walk through the n domains of coherent fields traversed by the path. In Table 1 we indicate the cosmic magnetic fields [23] and their coherence lengths, inferred from observations of synchrotron radiation and Faraday rotation, and from modeling. The typical values of the monopole kinetic energies that result from these fields are also shown in the Table. A similar table has been constructed in ref. [24].

If the early universe dynamics that generated these fields and/or the present dynamics that maintain these fields were known, then new Parker–like bounds could be placed upon the extragalactic monopole flux. With our limited knowledge at present, efforts in this direction (latter references in [4]) are highly model–dependent.

The largest energies are seen to come from the magnetic fields having the longest coherence lengths. The strength of these sheet fields is inferred from simulations [25] and observations [26]. It is anticipated that in the near future more reliable inferences of the extra-galactic magnetic fields will become available [28,31]. This will allow a firmer prediction of monopole energies.

We emphasize that a typical monopole which travels through the Universe, and has a mass below the energies indicated in Table 1, should be relativistic. Monopoles will gain and lose energy as they random–walk through the Universe, eventually producing a broad distribution of energies (with $\Delta E_K/E_K \sim 1$) centered roughly on $\sqrt{n}$ times the typical energy for a single transit through a region of homogeneous magnetic field. Here, n is the number of coherent fields encountered in the random walk. For extragalactic sheets, which we expect to dominate the spectrum, this number can be roughly estimated to be of order $n \sim H_0^{-1}/50\,\text{Mpc} \sim 100$. The resulting $E_{\max}$ is therefore estimated to be $\sim 10^{25}$ eV. Hence, monopoles with mass below $\sim 10^{14}$ GeV are expected to be relativistic. This is a fundamental result. The rest of this paper is devoted to the novel phenomenology of relativistic monopoles. We begin with a discussion of the interactions of monopoles with matter in the next section, and subsequently calculate monopole signatures in various detectors.

	B/μG	ξ/Mpc	$gB\xi$/eV	Refs.
normal galaxies	3 to 10	10^{-2}	$(0.3 \text{ to } 1) \times 10^{21}$	[27]
starburst galaxies	10 to 50	10^{-3}	$(1.7 \text{ to } 8) \times 10^{20}$	[28]
AGN jets	~ 100	10^{-4} to 10^{-2}	$1.7 \times (10^{20} \text{ to } 10^{22})$	[29]
galaxy clusters	5 to 30	10^{-4} to 1	3×10^{18} to 5×10^{23}	[30]
Extragal. sheets	0.1 to 1.0	1 to 30	1.7×10^{22} to 5×10^{23}	[25]

TABLE I. Estimated magnetic field strength and coherence length for some astrophysical environments, and the associated monopole energies for a single transit through the regions.

III. RELATIVISTIC MONOPOLE ENERGY LOSS IN MATTER

GUT monopoles are formed in non-trivial representations of $SU_C(3) \times SU_L(2) \times U_Y(1)$ and couple to the standard model gauge fields. An accurate description of the monopole stopping power must include all of the standard model interactions or the relevant subset of those interactions for the type of monopole considered. In this paper we choose to ignore the weak interaction throughout, which is suppressed in amplitude by factors $\sim M_Z^{-2}$. The electromagnetic and strong interactions will be accounted for in this section.

The strong interaction of a monopole is difficult to assess. Color confinement ensures that all observable monopoles are color singlet objects, and so have no classical long–range color–magnetic field. Nevertheless, we expect l–monopoles and baryonic–monopoles to have very different hadronic interactions. Although l–monopoles are fundamental and lack a color–magnetic charge, the unbroken symmetry in their core ensures that gluon and light quark fields will leak out from the center to the confinement distance $\Lambda_{QCD}^{-1} \sim 1$ fm [32]. In this way, l-monopoles will exhibit some hadronic cross-section in small impact-parameter scattering. This is probably ignorable. On the other hand, baryonic–monopoles are intrinsically hadronic in all partial waves.

We will resume the discussion of the monopole's strong interaction with hadronic matter after first discussing in some detail their better–understood electromagnetic interactions. The electromagnetic interaction of the monopole may dominate the hadronic interaction because the electromagnetic coupling of the monopole is large [33],

$$\alpha_M = \frac{1}{4\alpha} \simeq 34\,, \tag{3.1}$$

and mediated by a long–range field. At large distances and high velocities, the magnetic monopole with Dirac charge mimics the electromagnetic interaction of a heavy ion of charge $Z \sim \sqrt{\alpha_M/\alpha} \sim \frac{1}{2\alpha} \simeq 68$. We will follow others and treat the electromagnetic interaction of the monopole with matter semi–classically, i.e., viewing the monopole as a classical source of radiation, while treating the matter–radiation interaction quantum–mechanically. In this way, the large electromagnetic coupling of the monopole is isolated in the classical field, and the matter–radiation interaction can be calculated perturbatively [34].

The value of α_M given here, and conservatively used throughout this paper, is the minimal value due to Dirac. Other monopole solutions have charges which are integer multiples of the Dirac charge, and therefore α_M's which are larger by a factor of n^2, $n = 1, 2, 3, \ldots$. For example, the Schwinger solution and the original t'Hooft-Polyakov monopole have twice the Dirac charge, and an α_M that is four times minimal.

A. Electromagnetic Interactions

We consider here the energy losses of the monopole due to the four electromagnetic processes: ionization resulting from collisions with atomic electrons, e^+e^- pair production, bremsstrahlung, and the photonuclear interaction. It will be the pair production and photonuclear interactions, that dominate the energy loss for very large $\gamma \equiv E/M$ and will be mostly responsible for the growth of a particle shower. The monopole-matter electromagnetic interaction for $\gamma < 100$ is well reported [35,36] for atomic excitations and ionization losses in the absorber, including the density–dependent suppression effect arising from charge–polarization of the medium [37]. In the literature these two effects are collectively referred to as "collisional" energy losses and we follow that nomenclature.

It is convenient to express the energy loss per "length" in units of column density (g/cm^2) which we use throughout this work. The conversion from true length increment dL to column density increment dx is $dL = dx/\rho_N = (\frac{N_A}{g})(\frac{Z}{A\,n_e})\,x$, the latter form arising from writing the nuclear matter–density ρ as $m_N\,n_N$, and identifying the nucleon mass m_N and density n_N with the first and second fractions, respectively. In conventional notation, N_A is Avogadro's number, Z and A are the mean nuclear charge and number, n_e is the electron density, and g is the gram unit. We absorb the mass into A, giving A the units of grams per mol.

One approach to electromagnetic interactions is to replace the monopole current with an equivalent photon flux, $dN_\gamma/d\omega = 2\alpha_M/\pi\omega \ln(m\gamma/\omega)$, with m being the target mass and ω the photon energy in the rest frame. The equivalent photon approximation (EPA) is strictly valid for limited perpendicular momentum transfer $q_\perp \ll m$, and limited energy transfer $\omega \ll m\gamma$ [38]. Consequently, we prefer to use the more exact monopole–target scattering formula. Nevertheless, the EPA presents two illuminating features, the $1/\omega$ bremsstrahlung–type of photon spectrum, and the large normalization $2\alpha_M\pi = 1/2\pi\alpha \approx 22$. The latter tells us that electromagnetic cross–sections are large, while the former, in conjunction with $\omega \ll m\gamma$, shows that energy transfers are soft.

1. Collisional Energy Loss

The magnetic monopole stopping power formula calculated by Ahlen [36] includes ionization of the absorber at small impact parameters and atomic excitation at large impact parameters. For highly relativistic monopoles we may ignore the various correction terms and simply describe ionization with

$$\frac{dE_{\text{coll}}}{dx} = -\frac{4\pi Z\alpha\alpha_M N_A}{A m_e}\left[\ln\left(\frac{m_e\beta^2\gamma^2}{I}\right) - \frac{\delta}{2}\right]. \tag{3.2}$$

m_e is the electron mass, I is the mean charge and ionization energy of the material, and δ parameterizes the density effect [39].

2. Pair Production

A thorough study of pair production for muons [40] is adapted here for the case of a monopole. To accurately calculate shower development resulting from pairproduction the inelasticity must be understood. For a relativistic monopole primary the energy loss to pair production is

$$\frac{dE_{\text{pair}}}{dx} \simeq -\frac{16}{\pi}\frac{\alpha^3\alpha_M Z^2 N_A}{A m_e}\gamma\left(\frac{M}{m_e}\chi\right), \tag{3.3}$$

where

$$\chi \equiv \sum_{i=1}^{5}\chi_i, \tag{3.4}$$

$$\chi_i = \int_{\eta_{\min}}^{\eta_{\max}} d\eta\, F_i(\gamma, \eta), \tag{3.5}$$

the inelasticity, or fraction of monopole energy transferred in the interaction, is $\eta \equiv \Delta E/E$, and the five functions $F_i(\gamma, \eta)$ (given in [40]) are labeled by the five distinct regions of inelasticity and nuclear–charge screening:

$$
\begin{array}{clll}
1) & \text{slow pairs, no screening,} & \frac{2m_e}{\gamma M} < \eta < \frac{2m_e}{M} \\[4pt]
2) & \text{slow pairs, total screening,} & \frac{2m_e}{\gamma M} < \eta < \frac{2m_e}{M} \\[4pt]
3) & \text{fast pairs, no screening,} & \frac{2m_e}{M} < \eta < \frac{\gamma}{\frac{M}{m_e}+\gamma} & \text{(3.6)} \\[4pt]
4) & \text{fast pairs, no screening,} & \frac{\gamma}{\frac{M}{m_e}+\gamma} < \eta < 1 \\[4pt]
5) & \text{fast pairs, total screening,} & \frac{2m_e}{M} < \eta < 1.
\end{array}
$$
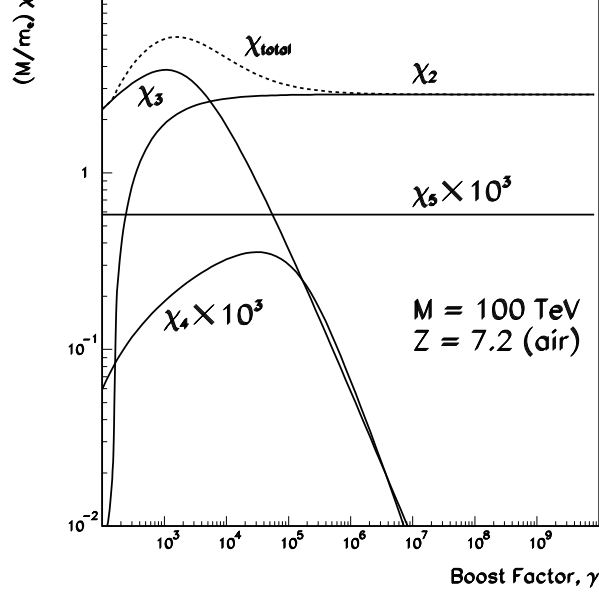
FIG. 1. Electron–pair production of an $M = 100$ TeV relativistic monopole in air is described in terms of the functions χ_i derived in [40]. The χ_i's relate to different regions of inelasticity space and either total or no screening.

In fig. (1) we plot the factors $\frac{M}{m_e}\chi_i$ versus γ to examine the relative strengths of the χ_i's. To a good approximation, pair production is proportional to the sum of just χ_2 and χ_3. The expression χ_1 is unphysical over the range of γ plotted while χ_4 and χ_5 have been multiplied by 10^3. For $M \gg m_e$, and keeping mass corrections with the largest powers of $\frac{m_e}{M}\ln^n\left(\frac{M}{m_e}\right)$, the no screening limit is

$$
\frac{dE_{\text{pair}}}{dx} \simeq -\frac{19\pi}{9}\frac{\alpha^3\alpha_M Z^2 N_{\text{A}}}{A m_e}\,\gamma\left[(1-B_1)\ln\left(\frac{\gamma}{4}\right) - B_2\right], \tag{3.7}
$$

and the total screening limit is

$$
\frac{dE_{\text{pair}}}{dx} \simeq -\frac{19\pi}{9}\frac{\alpha^3\alpha_M Z^2 N_{\text{A}}}{A\,m_e}\,\gamma\left[(1-B_1)\ln\left(\frac{189}{Z^{1/3}}\right) + \ln 2 - B_3\right], \tag{3.8}
$$

where

$$
\begin{aligned}
B_1 &= \tfrac{48}{19\pi^2}\tfrac{m_e}{M}\ln^2\left(\tfrac{M}{m_e}\right) \\
B_2 &= \tfrac{11}{6} - \tfrac{16}{19\pi^2}\tfrac{m_e}{M}\ln^3\left(\tfrac{M}{m_e}\right) \\
B_3 &= \tfrac{1}{38} + \tfrac{16}{19\pi^2}\tfrac{m_e}{M}\ln^3\left(\tfrac{M}{m_e}\right).
\end{aligned}
\tag{3.9}
$$

For $E \gg M \gg m_e$ as here, the contributions of the three B_i to eqs. (3.7) and (3.8) are negligible. Examination of fig. (1) shows that for $\gamma \gtrsim 10^5$, a total screening process dominates, meaning that eq. (3.8) describes the pair production energy loss.

3. Monopole Bremsstrahlung

Bremsstrahlung radiation by a relativistic particle in collision is inversely proportional to its mass, so we expect bremsstrahlung to be negligible for massive monopoles. The approximate stopping power due to brehmsstrahlung losses has been calculated [41] for electric charges in the negligible nuclear–screening limit [42]. For monopoles it is

$$\frac{dE_{\rm rad}}{dx} \simeq -\frac{16}{3} \frac{\alpha \alpha_M^2 Z^2 N_{\rm A}}{A\,M} \gamma \, \ln(\gamma). \tag{3.10}$$

4. Monopole Photonuclear Interaction

Virtual photon exchange between a monopole and a nucleus is described by the photonuclear cross–section. This process is $MN \rightarrow MX$, where M is a monopole, N a nucleus, and X are final state hadrons. The energy loss of leptons via the photonuclear interaction has been re-evaluated recently [43] in light of the HERA results for real and virtual photon–nucleon scattering. A full range of momentum transfer is accounted for from real $(Q \rightarrow 0)$ photon exchange to highly virtual photon–nucleon interactions. This analysis is adapted to monopoles with the replacements $m_\mu \rightarrow M$ and $e \rightarrow e/2\alpha$ where m_μ, M are the muon and monopole masses, respectively. For $\gamma > 10^6$ the photonuclear energy loss dominates pair production and the calculations, based on [43], give roughly $dE/dx \propto \gamma^{1.28}$.

B. Total Electromagnetic Losses

We collect the electromagnetic energy loss processes together and plot them in fig. (2) for $M = 100$ TeV monopoles. The dominant interactions are atomic collisions for $\gamma < 10^4$, pair production for $10^4 < \gamma < 10^6$, and photonuclear for $\gamma > 10^6$.
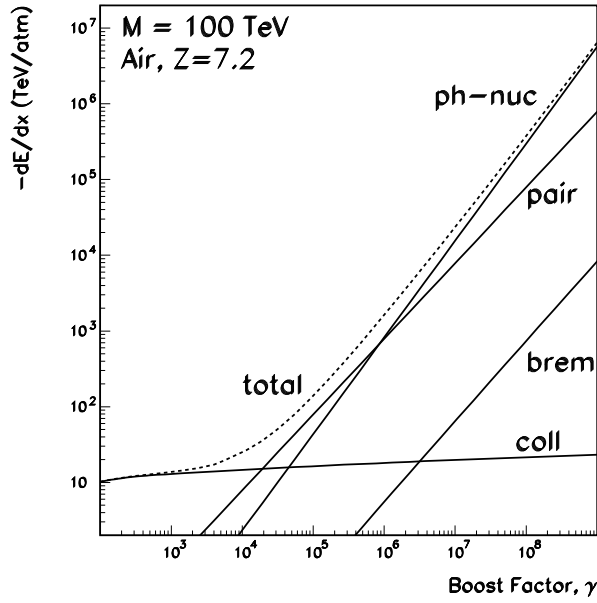
FIG. 2. The electromagnetic energy loss from collisional, bremsstrahlung, electron–pair production, and the photonuclear interaction of a 100 TeV relativistic monopole in air. Collisional, pair production, and the photonuclear interaction are roughly independent of the monopole mass whereas bremsstrahlung is $\propto M^{-1}$. The units of energy loss are given in TeV per atmosphere, where $1\,\mathrm{atm} = 1033\,\mathrm{g/cm^2}$.

C. Hadronic Interactions

GUT monopoles typically contain internal color fields. The l-monopole's color field is soft, extending to a distance $\Lambda^{-1} \sim 1$ fm (where $\Lambda \equiv \Lambda_{QCD}$). Its internal color is similar to that of a normal hadron, however there are no valence quarks internally, and so a better analogy to the color structure of an l-monopole is a glueball. Thus, we expect the hadronic cross–section of l-monopoles to be of typical hadronic size, with an inelasticity $\eta \sim \Lambda/M \sim 10^{-10}\,(10^{10}\mathrm{GeV}/M)$. For l–monopoles an approximate hadronic stopping power would then be

$$\frac{dE_{\mathrm{had}}}{dx} \simeq -\frac{\gamma\,\Lambda}{\lambda} \simeq -\gamma\,\Lambda\,\left(\frac{N_{\mathrm{A}}}{\mathrm{gram}}\right)\,\sigma_{\mathrm{had}} \tag{3.11}$$

where the mean–free–path between hadronic interactions is $\lambda = (N_{\mathrm{A}}\sigma_{\mathrm{had}})^{-1}$, for a typical hadronic cross–section σ_{had}. The magnitude of expression (3.11) appears to be comparable to the energy loss to electron–pairs discussed above, so the hadronic interaction for l-monopoles may make a significant contribution to the total energy loss. Lacking reliable knowledge of the l-monopole's hadronic interactions, we will neglect this possible contribution in the following signature calculations. In passing we mention that: 1) The inclusion of eq. (3.11) in the longitudinal shower model (sec. IV) would feed the electromagnetic shower. For each hadronic interaction length in the development of a subshower, about 30% of the hadronic energy is transferred to the electromagnetic component; thus, after a subshower undergoes a few hadronic interactions, $\mathcal{O}(1)$ of the energy will be in the electromagnetic shower. 2) The range of mass

11

for which monopole tomography (to be discussed in in sec. (IV D)) is viable will be shifted toward higher mass with the inclusion of eq. (3.11).

The baryonic–monopoles are quite different. In section (V) we develop a model for the energy loss of baryonic–monopoles. The QCD string model, where the total cross–section grows with string length l, describes baryonic-monopole hadronic interactions, with the significant caveat that the confining strings in the monopole are readily stretched but not easily broken. The energy loss is estimated to be

$$\frac{dE_{\text{had}}}{dx}(x) \simeq -\frac{\gamma\,\Lambda}{\lambda(x)} \simeq -\gamma\,\Lambda\left(\frac{N_{\text{A}}}{\text{gram}}\right)\sigma(x) \simeq -\gamma\left(\frac{N_{\text{A}}}{\text{gram}}\right)l(x)\,, \tag{3.12}$$

where the string cross–section $\sigma(x) = l(x)\Lambda^{-1}$ is explicitly a function of column depth x.

IV. MONOPOLE ELECTROMAGNETIC SIGNATURES

Signature events for l-monopoles are derived below with a specific emphasis on 1) the general shower development, 2) Cherenkov signatures, 3) the nitrogen fluorescence signature, and 4) Earth tomography. The general shower characteristics are developed first as the other signatures are derivable from that model. For the remainder of this section we only consider l-monopoles, which we will simply refer to as "monopoles".

A. Monopole Shower Development

Monopoles will be highly penetrating primaries. On average, there will be a quasi-steady cloud of secondary particles continuously regenerated along the monopole trajectory. Thus, we will call this type of shower "monopole–induced," in contrast to conventional particle–initiated showers.

1. Monopole–Induced Subshowers

Given a fast monopole passing through matter, the various electromagnetic processes discussed in sec. (III) can inject energetic photons, electrons, and positrons into the absorbing medium. If the energy of these injected secondary particles is sufficient, they may initiate a particle cascade. In the simple model we consider, originally developed by Heitler [44] and reviewed in [45,46], the photon pair production length is set equal to the electron (or positron) radiation length. Consider a photon primary of initial energy E_0 which travels a mean distance R through the absorber before pair producing [47]. The two particles in the produced pair are assumed to share equally the initial photon's energy. After traveling another distance R the electron and positron each radiate a bremsstrahlung photon where the produced photon takes half the parent energy. The particle number has doubled again and the energy per particle is halved again. The shower continues to develop in this geometric fashion until the energy per particle drops to the critical energy, E_c, below which ionization of the absorber dominates the energy losses due to particle–production processes. For typical materials, $E_c \simeq 100$ MeV.

From the relation for energy per particle,

$$E(x) = E_0\,\mathrm{e}^{-\frac{x}{\xi_e}}\,, \tag{4.1}$$

it is apparent that R is related to the radiation length ξ_e by $R = \xi_e \ln 2$. The number of particles in the shower at a given depth is approximately

$$N(x) = e^{\frac{x}{\xi_e}} . \tag{4.2}$$

The maximum number produced is $N_{\max} = \frac{E_0}{E_c}$, from which we infer the depth of the shower maximum to be

$$X_{\max} = \xi_e \ln \left(\frac{E_0}{E_c} \right) . \tag{4.3}$$

After reaching the shower maximum at $X_{\max}$, the shower size decreases with column depth as a relativley mild exponential. The value of ξ_e in air is quoted as $34\,\mathrm{g/cm^2}$ [46], while the value in ice is quoted as $36\,\mathrm{g/cm^2}$ [50]. The slight dependence on composition reflects the small differences in mean charge of the nuclei. The attenuation length for the post-$X_{\max}$ decay is approximately $200\,\frac{\mathrm{g}}{\mathrm{cm^2}}$ [51], or about $6\,\xi_e$.

2. Longitudinal Shower Profile

It is straightforward to qualitatively describe the electromagnetic shower from pair production. The subshowers begin their existence as an e^+e^- pair, produced nearly at rest in the cms. The subshower energy is therefore $\sim 2m_e$ boosted to the lab frame. Since M is much greater than the nucleon mass, the cms frame is nearly coincident with the monopole rest frame, and we have $E_0 \sim 2\gamma m_e$ for the subshower energy. The electromagnetic process by which the subshower repeatedly cascades, and the process by which the monopole initiates the subshower differ only by the attachment of the monopole to a photon line; i.e., the monopole interaction mean free path λ is a factor of $\frac{\alpha_M}{\pi}\frac{1}{\ln 2} \sim 16$ smaller than the subshower radiation length ξ_e. Each subshower attains its $N_{\max}$ and retains this particle number for roughly an attenuation length $6\,\xi_e$ (as presented above). Thus, the number of subshowers contributing to the steady–state shower size at any given moment is $6\,\xi_e/\lambda \sim 100$. With ~ 100 subshowers contributing to the total shower, we find $N \sim 100\,E_0/E_c \sim \gamma$ for the total particle number of the steady-state cloud accompanying the monopole. It is a pleasant coincidence that the proportionality in $N \sim \gamma$ is of order unity.

The electromagnetic shower produced by the photonuclear process is harder to estimate. This process dominates the total energy loss for $\gamma > 10^6$ and will dominate the fluorescence yield over that range, but it's contribution to the electromagnetic shower is indirect. In an Appendix we present a quantitative model for the electromagnetic shower from pair production and discuss the contribution from the photonuclear interaction. In fig. (8) shown later, we plot the shower size $N_{\max}$ versus γ based on the detailed shower model. It is reassuring to see the qualitative agreement between the detailed calculation and the approximate relation $N_{\max} \sim \gamma$ with its pleasing $\mathcal{O}(1)$ proportionality.

B. Monopole Cherenkov Signatures

When a charge travels through a medium with index of refraction n, at a velocity $\beta > \frac{1}{n}$, Cherenkov radiation is emitted [52]. The Frank-Tamm formula gives the total power emitted per unit frequency ν and per unit length l by a charge Ze,

$$\frac{d^2W}{d\nu\,dl} = \pi\alpha Z^2 \nu \left[1 - \frac{1}{\beta^2 n^2} \right] . \tag{4.4}$$

The maximal emission of the Cherenkov light occurs at an angle $\theta_{\max} = \arccos(1/n\beta)$ where θ is measured from the radiating particle's direction.

1. Direct Monopole Cherenkov Emission

The interaction of a magnetic charge with bulk matter requires the replacement of factors of ϵ with the Maxwell dual factors μ. But μ and ϵ are related by the index of refraction. The replacement the electric charge formulae, eq. (4.4) with $Z = 1$, adequate for magnetic monopoles is $\alpha \to n^2/4\alpha$, and leads to an enhancement factor of 4700 for monopoles interacting in vacuum and 8300 for monopole interactions in water. Cherenkov light from an electric charge source is linearly polarized in the plane containing the path of the source and the direction of observation. However, the light polarization from a magnetic charge will be rotated 90 degrees from that of an electric charge which, in principle, offers a unique Cherenkov signature for monopoles [53].

The direct Cherenkov signature of a monopole leads to the best experimental limits at present on the flux of relativistic monopoles. From the absence of a Cherenkov signal in deep water PMTs the Baikal Collaboration reports the limit $F_M \overset{<}{\sim} 6 \times 10^{-16}/\text{cm}^2/\text{s/sr}$ [54], while the absent signal in deep ice translates into the AMANDA limit $F_M \overset{<}{\sim} 1.6 \times 10^{-16}/\text{cm}^2/\text{s/sr}$ [55]. There is a comparable limit of $F_M \overset{<}{\sim} 4 \times 10^{-16}/\text{cm}^2/\text{s/sr}$ obtained by the MACRO collaboration using scintillators and streamer tubes [56]. Note that these limits are already slightly more restrictive than the Parker limit. This work shows that the direct Cherenkov signal in the optical should be swamped by the electromagnetic shower for monopoles with $\gamma > 10^5$ (see fig. (6)). Such a signal is not seen by AMANDA [57] and so the AMANDA monopole flux limit remains the same as that derived from the non-observation of a direct Cherenkov signal. In sec. (IV D) we calculate that relativistic monopoles can pass through a large portion of the earth for $M \overset{>}{\sim} 3$ PeV. Given this result, any experimental limit for upgoing relativistic monopoles should only apply roughly in the mass range $M \overset{>}{\sim} 3$ PeV.

2. Coherent Radio–Wavelength Cherenkov Emission

In addition to the Cherenkov radiation from the bare monopole charge there is a contribution from the relativistic e^+–e^- cascade comprising the shower. Therefore, an estimation of the total power radiated in Cherenkov light requires the model developed above for the size of the monopole induced shower.

The approximate lateral width of a monopole-induced cascade is given by the Molière radius (7.15) which means the excess electric charge [58] is confined roughly within a distance R_M. Cherenkov light of wavelength $\lambda \gg R_M$ emitted by the monopole-induced shower will be radiated coherently and be strengthened by the Z^2 factor in eq. (4.4). Simulations of electromagnetic showers in ice [50] show that the cascade contains an electric charge excess of about 20% the total shower size. This is plotted for ice in figure (8).

The proposed Radio Ice Cherenkov Experiment (RICE) may offer the best chance for the detection of monopoles in a 1km^3 scale detector resulting from the transparency of ice in the radio. [59] A thorough study, on a par with that done for high energy neutrinos [60], has not been undertaken for monopoles in RICE. In lieu of such a study we remark that the most noticeable signature should be that the monopole is highly penetrating and will traverse the full

detector size without an appreciable loss of kinetic energy. Thus, the monopole signature is easily distinguished from a neutrino event, which is a localized shower that produces a Cherenkov cone detectable only by a limited number of antennae lying within the cone. Timing can be used to reconstruct the monopole path.

The analysis of neutrino energy thresholds at RICE can be used to estimate an energy threshold for monopole events. Figure (13) in [60] can be interpreted for *monopole* detection as showing that an effective volume of 1km^3 per antenna is reached if $dE/dx \stackrel{>}{\sim} dE_{\text{th}}/dx \approx 3 \times 10^{12} \,\text{eVcm}^2/\text{g} \approx 3 \times 10^3 \,\text{TeV/atm}$. This translates into a threshold boost factor, read off from figure (2), of $\gamma \stackrel{>}{\sim} \gamma_{\text{th}} \approx 10^6$. For a RICE monopole search to have an effective volume $\stackrel{>}{\sim} 1 \text{km}^3$ the monopole boost is restricted to $\gamma \stackrel{>}{\sim} 10^6$.

The monopole flux limits which RICE could set are much stronger than those currently available (Baikal, AMANDA, or MACRO [54–56,61]). A year of observation in the km^3 RICE detector without a candidate monopole event would set a flux limit at least as good as $10^{-18} \,\text{cm}^{-2}\text{sec}^{-1}\text{sr}^{-1}$, three orders of magnitude below the Parker bound and two orders of magnitude better than the current bounds.

C. Monopole Fluorescence Signatures

A sensitive probe of high energy air shower development is the nitrogen fluorescence emitted by the atmosphere. The Fly's Eye and HiRes experiments have fruitfully pioneered this technique. The yield in nitrogen fluorescence is $\sim 0.5\%$ times the total energy in ionization of the atmosphere. Since $\mathcal{O}(1)$ of the energy loss by all processes ends up in ionization of the atmosphere once the subshowers have ranged out, we need to evaluate the total stopping power to estimate the fluorescence yield. The total energy loss is the sum of the various processes summarized above:

$$\frac{dE_{\text{total}}}{dx} = \frac{dE_{\text{coll}}}{dx} + \frac{dE_{\text{pair}}}{dx} + \frac{dE_{\text{rad}}}{dx} + \frac{dE_{\gamma-\text{nuc}}}{dx} + \frac{dE_{\text{had}}}{dx}. \tag{4.5}$$

For l-monopoles the electromagnetic energy loss dominates, and in a thin absorber like the atmosphere, l–monopole energy deposition is typically below threshold [62]. For light l-monopoles at extreme γ, photonuclear losses dominate and

$$\frac{dE_{\text{total}}}{dx} \approx -10^6 \, \frac{1}{\cos\theta_Z} \, \left(\frac{Z}{7.2}\right)^2 \left(\frac{14.4}{A}\right) \left(\frac{\gamma}{10^8}\right)^{1.28} \frac{\text{TeV}}{\text{atm}}. \tag{4.6}$$

On the other hand, baryonic–monopoles [22] interact such that $\frac{dE_{\text{had}}}{dx}$ dominates the total energy loss. For baryonic–monopoles a large energy transfer to the atmosphere is natural. In section (V) a model for the baryonic–monopole interaction is developed.

D. Earth Tomography with Relativistic Monopoles

Direct knowledge about the composition and density of the Earth's interior is lacking. Analysis of the seismic data is currently the best source of information about the Earth's internal properties [64,65]. However, another potential probe would be the study of highly penetrating particles interacting with the Earth's interior. With such a means it may be possible to directly measure the density profile of the Earth's interior [66]. Here we show that over a range of initial kinetic energies monopoles can pass through the Earth's interior and emerge with relativistic velocities. The

15

results of a numerical calculation, making use of the full energy loss expressions derived earlier and a simple model approximating the internal composition of the Earth, are described below. Our calculation shows that relativistic monopoles in the $3 \to 10$ PeV (1 PeV $= 10^{15}$ eV) mass range are ideal for Earth tomography, and that monopoles may pass through the Earth to initiate up–going cosmic ray events.

1. Two Shell Earth Model

Dziewonski and Anderson [67] have developed the preliminary Earth reference model (PREM) which is the standard Earth model in use today. The PREM model consists of eight concentric shells of varying density and composition. It is sufficient for the purpose of demonstrating monopole tomography to simplify this model to two shells, the mantle and the core [68]. Both shells are taken to be spherically symmetric. The core has a radius $R_{\text{core}} = 3.486 \times 10^6$ m and a mean mass density $\rho_{\text{core}} = 11.5 \frac{\text{g}}{\text{cm}^3}$. The mantle extends from the core out to the earth's surface at $R_\oplus = 6.371 \times 10^6$ m and has a mean mass density $\rho_{\text{mantle}} = 4.0 \frac{\text{g}}{\text{cm}^3}$. We take both shells to be of uniform composition. The chemical composition of the mantle (in mass) is approximated by SiO_2 (45.0%), Al_2O_3 (3.2%), FeO (15.7%), MgO (32.7%), and CaO (3.4%), and that of the core is approximated by Fe (96.0%) and Ni (4.0%) [69]. From these data we calculate the chemical composition (in percentage of *molecular type*) for the mantle as SiO_2 (40.0%), Al_2O_3 (1.67%), FeO (11.6%), MgO (43.6%), and CaO (3.23%), and for the core as Fe (96.2%) and Ni (3.8%).

The electromagnetic energy loss processes for relativistic monopoles were analyzed in sec. (III). The energy loss formulae contain various parameters which need to be specified for the core and mantle of the Earth. The density effect includes the following dimensionful parameters:

the plasma frequency [36]

$$\omega_p \simeq \left\{ \begin{array}{ll} 66.2 \text{ eV} = 3.36 \times 10^6 \text{cm}^{-1} & \text{(core)} \\ 40.4 \text{ eV} = 2.05 \times 10^6 \text{cm}^{-1} & \text{(mantle)} \end{array} \right\}, \tag{4.7}$$

and the mean ionization potential [36]

$$I \simeq \left\{ \begin{array}{ll} 285 \text{ eV} & \text{(core)} \\ 172 \text{ eV} & \text{(mantle)} \end{array} \right\}; \tag{4.8}$$

and various numbers in the Sternheimer and Peierls parameterization [39]:

$$C \equiv -2\ln\left(\frac{I}{\omega_p}\right) - 1 \simeq \left\{ \begin{array}{ll} -3.92 & \text{(core)} \\ -3.90 & \text{(mantle)} \end{array} \right\}, \tag{4.9}$$

$$a \equiv -\frac{C + 4.606 X_0}{(X_1 - X_0)^3} \simeq \left\{ \begin{array}{ll} 0.137 & \text{(core)} \\ 0.136 & \text{(mantle)} \end{array} \right\}, \tag{4.10}$$

the latter obtained from $X_0 = 0.2$ and $X_1 = 3.0$ for both the core and the mantle. The functional form [39] for $\delta(\gamma)$ in the core is

$$\delta^{\text{core}}(\gamma) \simeq \left\{ \begin{array}{ll} 0 & \gamma < 1.87 \\ -3.92 + \ln(\gamma^2 - 1) + 0.0297\left[13.82 - \ln(\gamma^2 - 1)\right]^3 & 1.87 < \gamma < 1000 \\ -3.92 + \ln(\gamma^2 - 1) & 1000 < \gamma \end{array} \right\}, \tag{4.11}$$

and in the mantle is

$$\delta^{\text{mantle}}(\gamma) \simeq \begin{cases} 0 & \gamma < 1.87 \\ -3.90 + \ln(\gamma^2 - 1) + 0.0295 \left[13.82 - \ln(\gamma^2 - 1)\right]^3 & 1.87 < \gamma < 1000 \\ -3.90 + \ln(\gamma^2 - 1) & 1000 < \gamma \end{cases}. \tag{4.12}$$

Lastly, the mean nuclear charges and mean atomic weights, calculated from the chemical compositions given above, are

$$\bar{Z} \simeq \begin{cases} 26.1 & \text{(core)} \\ 10.8 & \text{(mantle)} \end{cases}, \tag{4.13}$$

$$\bar{A} \simeq \begin{cases} 56.1 \text{ grams/mol} & \text{(core)} \\ 21.7 \text{ grams/mol} & \text{(mantle)} \end{cases}. \tag{4.14}$$

2. Numerical Results

We integrate $\frac{d\gamma(x)}{dx} \equiv \frac{1}{M} \frac{dE(x)}{dx}$ to find the final boost factor for the monopole after traversing the earth. The input parameters are the monopole mass and initial boost factor. The results are plotted in figure (4). The figure shows several curves with different initial kinetic energies, for a fixed monopole mass.
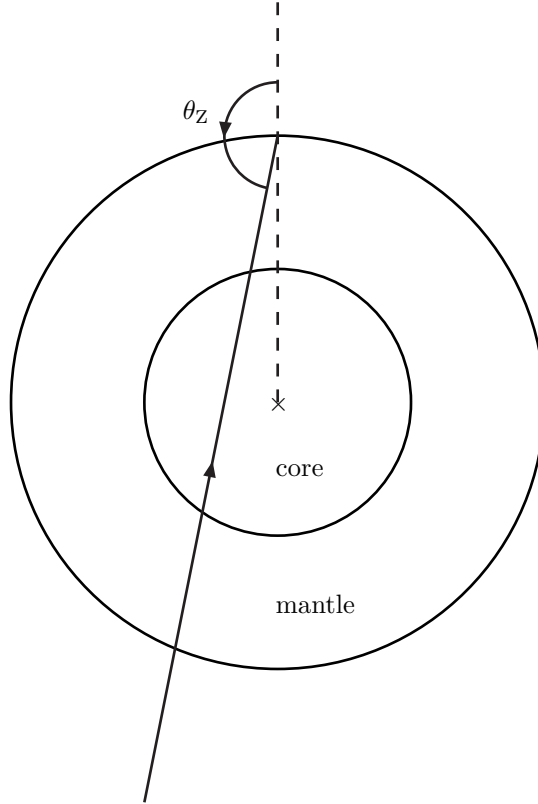

FIG. 3. A schematic representation of earth tomography with a highly penetrating particle. Monopole energy losses differ in passing through the core or mantle and so affect the energy spectrum of upcoming monopoles as a function of zenith angle θ_Z. For a zenith angle $\theta_Z^{\text{core}} \simeq 147°$, the upcoming particle grazes the edge of the core.

17

The initial energy spectrum can be determined from the $\theta_Z \leq \frac{\pi}{2}$ data. These monopoles have not passed through the earth and therefore retain the original kinetic energy attained from the large-scale magnetic fields. A comparison of these data with the $\theta_Z > \frac{\pi}{2}$ data could make a determination of the earth's interior possible. In figure 4, the discontinuity due to the mantle–core boundary is clear [70]. The zenith angle for a trajectory tangent to the core boundary is

$$\theta_Z^{\mathrm{core}} = \pi - \arcsin\left(\frac{R_{\mathrm{core}}}{R_\oplus}\right) \simeq 147°. \tag{4.15}$$

Assuming that $\mathcal{O}(100)$ data points would be sufficient to delineate the attenuation curves of figure 4 we can estimate the detector exposure needed in the 2π steradians projected through the Earth:

$$t = 1\,\mathrm{year}\,\frac{1}{2\pi}\left(\frac{\mathrm{N}}{100}\right)\left(\frac{10^{-16}/\mathrm{cm}^2\,\mathrm{sec\,sr}}{\mathrm{F_M}}\right)\left(\frac{1\mathrm{km}}{\mathrm{R}}\right)^2. \tag{4.16}$$

The monopole flux $F_\mathrm{M} \approx 10^{-16}/\mathrm{cm}^2\,\mathrm{sec\,sr}$ is roughly the experimental upper bound of [54–56].
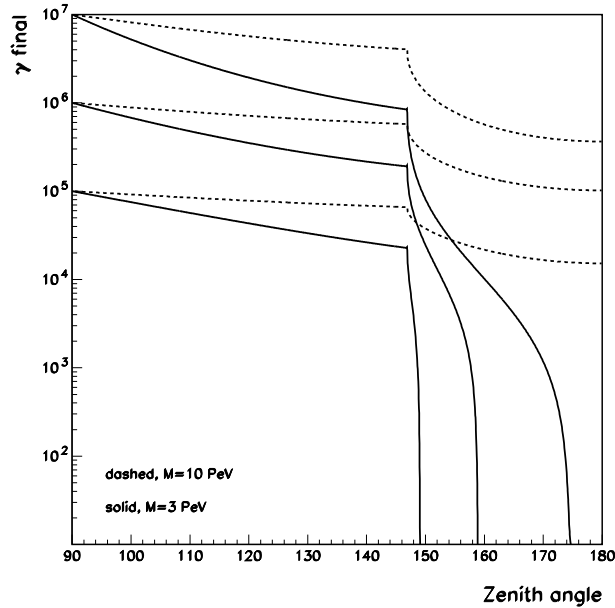

FIG. 4. $M = 3 \times 10^{15}$ and $M = 10^{16}$ eV monopoles passing through the earth and emerging with a diminished boost factor for increased zenith angle. The range of initial kinetic energies presented here is $3 \times 10^{20}\,\mathrm{eV} < \mathrm{E_M} < 10^{23}$ eV.

V. BARYONIC–MONOPOLE AIR SHOWERS AND SUPER–GZK EVENTS

The observation of air–showers above the GZK cutoff at $E_{GZK} \sim 5 \times 10^{19}$ eV presents a puzzle. These events cannot be due to nucleons or photons propagating from sources located at cosmic distances (see [6] for a recent discussion of the puzzling nature of these events). The natural acceleration of monopoles to energies above the GZK cutoff, and the allowed abundance of a monopole flux at the observed super–GZK event rate of $2.0 \pm 0.5 \times 10^{-20}/\mathrm{cm}^2/\mathrm{s/sr}$ above

10^{20} eV [71] (five orders of magnitude below the Parker limit), motivates us to ask whether monopoles may contribute to the observed super–GZK events. As a proof of principle, here we present a simple model of a baryonic–monopole interaction in air which produces a shower similar to that arising from a proton primary. (We note that an unrelated mechanism for mimicking a high–energy proton–initiated air shower with a monopole–nucleon bound state has been advanced in [24].) To mimic a proton–induced shower the monopole must transfer nearly all of its energy to the shower in a very small distance. The large inertia of a massive monopole makes this impossible if the strong cross–section is typical, ~ 100 mb [72]. The cross–section we seek needs to be much larger.
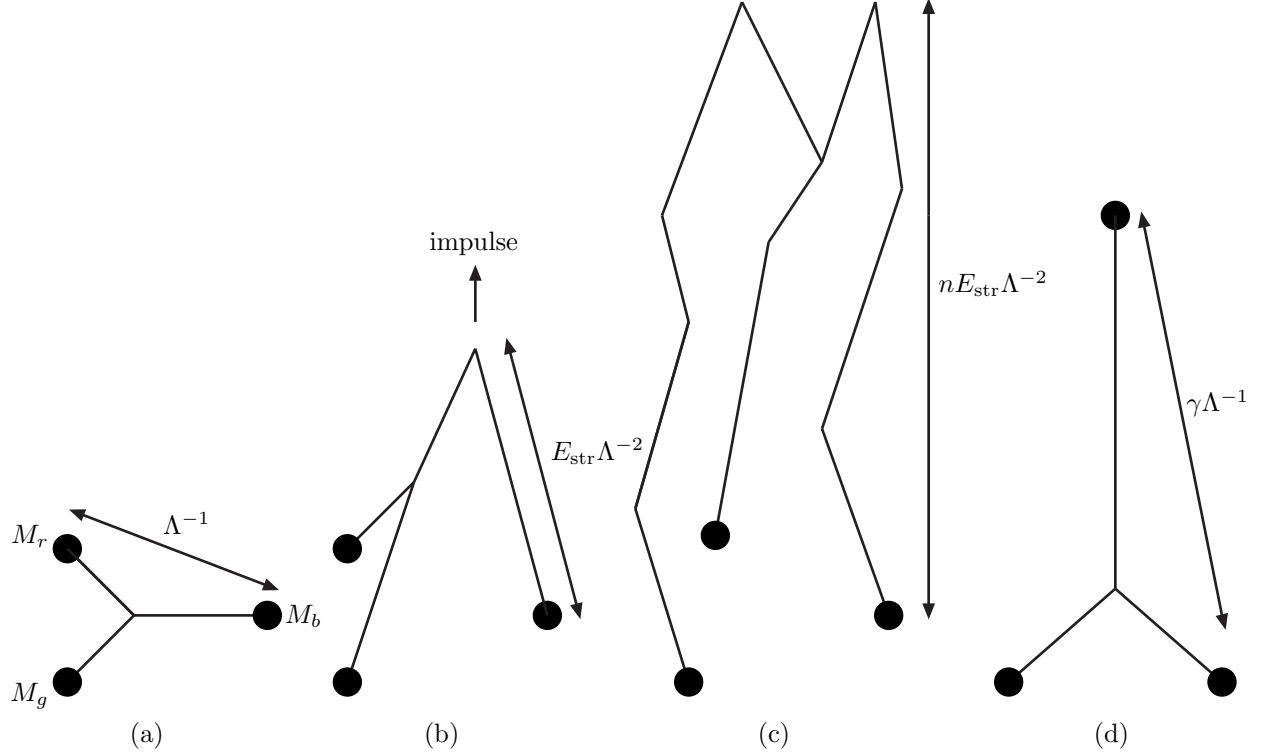

FIG. 5. A schematic representation of a baryonic–monopole interacting with the atmosphere that depicts the effect of string–nucleon interactions. Fig. (a) shows the baryonic–monopole in its unstretched state, before hitting the atmosphere. After the first string–nucleon interaction (fig. (b)) the string stretches to length $\sim E_{\mathrm{str}} \Lambda^{-2}$, and after n interactions (fig. (c)) it stretches to $\sim n E_{\mathrm{str}} \Lambda^{-2}$. Fig. (d) shows string stretching from q–monopole recoil.

We model our arguments on [22] where three $q-$monopoles are confined by Z_3 strings of color–magnetic flux to form a color–singlet baryonic–monopole as in figure (5a). All scales in the ground state baryonic-monopole are set by the QCD scale Λ. In particular, the string tension has the usual QCD-strength $\mu \simeq \Lambda^2$. We further assume that:

(1) Before hitting the atmosphere, the baryonic–monopole's cross–section is roughly hadronic, $\sigma_0 \sim \Lambda^{-2}$.

(2) Each interaction between the baryonic-monopole and an air nucleus transfers on average energy E_{str} (in the monopole rest-frame) into the chromomagnetic string system of the baryonic–monopole.

(3) Since the chromomagnetic strings can only be broken with the formation of a heavy $q-$monopole–antimonopole pair, the internal energy does not break the strings but rather stretches them by amount $\delta L = E_{\mathrm{str}}/\mu \simeq (E_{\mathrm{str}}/\Lambda)$ fm; the string system grows linearly with each interaction, until other emission processes of the stretched (and presumably

vibrating) string dominate [73].

(4) The cross–section for the interaction of the baryonic–monopole with a nucleus is geometric, $\sigma \sim L\Lambda^{-1}$, where L is the (growing) string length; this assumption says that string–nucleon interactions dominate over q–nucleon interactions.

(5) The energy emission rate from the excited string system (in the monopole frame) is proportional to some small power p of the (growing) string length (and therefore, to the same power of the number of hits and (growing) cross-section).

Together, the assumptions imply that the baryonic–monopole cross-section grows from typical hadronic at first interaction, $\sigma_0 \sim \Lambda^{-2}$, to

$$\sigma_n = L\Lambda^{-1} = n\,\frac{E_{\mathrm{str}}}{\Lambda^3} \tag{5.1}$$

after n interactions. A scematic drawing of the baryonic–monopole is given in figure (5) for (a) the ground state, (b) after the first interaction, and (c) after the nth interaction. This growth ($\propto L$) continues with each interaction, until finally the rising rate of particle emission $\dot{E}_{\mathrm{emit}}$ ($\propto L^p$) equals the rate of energy acquisition due to stretching. If $E_{\mathrm{str}} \gg \Lambda$, then already after the *first* interaction the cross–section is sufficiently large to shrink the subsequent interaction length to a small fraction of the depth of first interaction. This allows $\mathcal{O}(1)$ of the incident monopole energy to be transferred to the air nuclei over a short distance, just as in a hadron–initiated shower.

We can be more quantitative. The rate of internal energy acquisition effecting string–stretching exceeds the rising rate of particle emission as long as

$$\frac{E_{\mathrm{str}}}{\Delta t} > \dot{E}_{\mathrm{emit}}\,, \tag{5.2}$$

where Δt is the time between interactions in the monopole rest frame. Explicitly, we have

$$(\Delta t)^{-1} = \gamma\,(\Delta t_{\mathrm{lab}})^{-1} = \gamma\frac{c}{\lambda_{\mathrm{lab}}} = c\gamma\rho_N\sigma\,, \tag{5.3}$$

where ρ_N is the nucleon density of air in the lab frame. It is important to the model that the monopole first has a growing phase, and then before it becomes non-relativistic, the emission phase. This requires that inequality (5.2) hold for the initial interactions. Such will be the case when $p > 1$, i.e. the emission rate from the string grows nonlinearly with the string length. We comment on this below. Inputting eqs. (5.1) and (5.3) into (5.2), we find that the baryonic–monopole remains in its growth phase until the critical n^{th} interaction

$$n_{\mathrm{str}} = \frac{\Lambda^2}{E_{\mathrm{str}}}\left[\frac{E_{\mathrm{str}}}{\Lambda}\frac{c\gamma\rho_N}{\kappa(p)}\right]^{\frac{1}{p-1}}\,. \tag{5.4}$$

Here, $\kappa(p)$ is the proportionality constant in $\dot{E}_{\mathrm{emit}} = \kappa(p)L^p$. The "size" of the monopole at the conclusion of its growth phase is $\sigma_{n_{\mathrm{str}}} = n_{\mathrm{str}}E_{\mathrm{str}}/\Lambda^3$. (For our order of magnitude estimates, we benignly neglect the recoil of the monopole and the related decrease of γ with each interaction.) The distance between the first interaction and the onset of the emission phase is

$$\Delta X \sim \sum_{n=1}^{n_{\mathrm{str}}} \lambda_n\,, \tag{5.5}$$

which, according to $\lambda_n = \Lambda\lambda_0/E_{\mathrm{str}}n$, is

$$\Delta X \sim \frac{\Lambda}{E_{\text{str}}} \lambda_0 \sum_{n=1}^{n_{\text{str}}} \frac{1}{n} \; ; \tag{5.6}$$

λ_0 and λ_n are the mfp's of the monopole in the initial ground state and after n interactions, respectively, and the density of nucleons is taken here to be a constant for simplicity of illustration. The sum is a finite series, and for $n_{\text{str}} \gg 1$ is very nearly equal to $\ln(n_{\text{str}})$ [75], giving

$$\Delta X_{\text{str}} \sim \frac{\Lambda}{E_{\text{str}}} \lambda_0 \, \ln(n_{\text{str}}) \tag{5.7}$$

as the estimate for the total distance traveled by the baryonic–monopole in its growth phase. As derived here, ΔX and λ are lengths in the monopole rest-frame. However, our eqs. (5.5)–(5.7) are homogeneous in these variables, and so also apply in the Earth frame without change. In terms of column density of air, this distance is just

$$\Delta x_{\text{str}} = \frac{n_N}{N_A} \Delta X \sim 100 \left(\frac{\Lambda}{E_{\text{str}}} \right) \ln(n_{\text{str}}) \, \text{g/cm}^2 \,, \tag{5.8}$$

where the numerical value is evaluated in the Earth frame. Turning to the emission phase, equilibrium between absorption and emission fixes the average energy emitted per interaction to be $\sim E_{\text{str}}$ in the monopole frame. An energy M in the monopole frame, isotropically emitted, boosts to $\gamma M = E$ in the lab frame. Therefore, the number of interactions required to absorb and re-emit the energy observed as an air-shower is

$$n_{\text{emit}} \sim \frac{M}{E_{\text{str}}} \,. \tag{5.9}$$

Numbers are Lorentz invariants. Using $\lambda_{n_{\text{str}}} = \lambda_1 / n_{\text{str}} = \frac{\Lambda}{E_{\text{str}}} \frac{\lambda_0}{n_{\text{str}}}$ and eq. (5.7), the distance traveled in the emission phase is then

$$\Delta X_{\text{emit}} \sim n_{\text{emit}} \lambda_{n_{\text{str}}} = \frac{M\Lambda}{E_{\text{str}}^2} \frac{\lambda_0}{n_{\text{str}}} \,. \tag{5.10}$$

This too can be quite short compared to the mfp λ_0 of the ground-state monopole.

The two constraints on the model, that the length of the stretching phase ΔX_{str} and the length of the emission phase ΔX_{emit} be short compared to the mfp λ_0 for first interaction, can be written with the help of eqs. (5.7) and (5.10) as:

$$\frac{M\Lambda}{E_{\text{str}}^2} \ll n_{\text{str}} \ll e^{E_{\text{str}}/\Lambda} \,, \tag{5.11}$$

with n_{str} given by eq. (5.4). For a monopole mass of 100 TeV (10^{10} GeV), the left and right terms of the inequality are correctly ordered for $E_{\text{str}}/\Lambda > 10$ (20). Thus, for $E_{\text{str}} \gg \Lambda$, a broad range of n_{str} values will satisfy eq. (5.11). Furthermore, all values of n_{str} are available by suitably choosing the free parameter $\kappa(p)$. Thus, the model is natural in that it does not require fine–tuning of parameters. We have succeeded in constructing a stretchable chromomagnetic–string model for the baryonic–monopole which provides an existence proof that a very massive monopole, despite its inertia, may nevertheless transfer $\mathcal{O}(1)$ of its relativistic energy to an air shower over a very short distance. Such a monopole mimics the signature of a primary nucleon or nucleus. Of course, the last gasp of the monopole will not resemble a nucleon, for the monopole will eventually become non-relativistic and shed its internal energy more and more isotropically. If this "end game" energy is a small fraction of the air-shower energy, it will be difficult to observe.

Let us discuss assumptions (2), (3), and (5). Any assumption that does not violate known physics is valid until disproven by Nature. However, it is motivational to look for plausibility arguments. Assumption (2) states that

energy E_{str} per interaction stretches the string. An analogy to $p - p$ scattering may be illuminating here. The baryonic monopole contains a QCD energy of roughly Λ. Thus, the stong–interaction scattering dynamics bear some resemblance to $p - p$ scattering at $s \sim \gamma \Lambda m_N \sim (\mathrm{TeV})^2$. $p - p$ scattering data at 2 TeV cms energy are available from Fermilab's $p - \overline{p}$ Tevatron collider. A mainly diffractive QCD interaction stretches particle production throughout the rapidity plateau, emitting $\sim 10^2$ particles with typically $\sim$ few GeV energies. When a Z_3 string is struck by an air nucleus, the diffractive QCD dynamics may be similar, stretching the colored strings across the rapidity plateau. However, by assumption (3), the chromomagnetic string cannot break, and so a significant fraction of the $\mathcal{O}(100 \text{ GeV})$ energy remains in the stretched string, with the remaining energy materializing as light hadrons. The value $E_{\mathrm{str}} \sim \mathcal{O}(100 \text{ GeV})$, implying $E_{\mathrm{str}}/\Lambda \sim 10^3$, appears more than ample (by an order of magnitude or more) to sustain the model we have outlined. We also note that whereas the color-electric charge interactions are asymptotically free, the strength of the color-magnetic interactions increases with energy to preserve the Dirac quantization condition. This may further argue in favor of the non-breaking, coherent behavior of the chromomagnetic string.

Assumption (3) states that energy emission by the excited string is negligible in the early growth phase of the string. Some analogies may motivate this assumption. First of all, as is the case with a classical violin string, the Q of a resonating string (related to the decay time) can be very large compared to the time it takes to excite ("pluck") the string. Secondly, as is the case with cosmic strings, energy loss through particle emission may be inefficient until cusps or interconnections are formed. Assumption (5) states that the particle emission rate from the string grows nonlinearly with increasing L. We believe this is a reasonable expectation upon nature. E.g., the emission may occur as a result of string pinching to form cusps, or crossing to form reconnections, etc. The nonlinear nature of pinching and crossing is the reason these phenomena are studied numerically on a lattice, rather than analytically. Also, the QCD string is non-abelian, so that interactions among string sections are not linear. In fact, one may wonder whether our assumption (3), namely, *linear* string growth per interaction, is sensible. What really drives the model is that the baryonic–monopole cross–section grows rapidly upon interaction, and that the particle emission rate grows even more rapidly; linearity of the string growth, adopted in the model here for illustration, is not an essential aspect of the dynamics.

According to eq. (5.1), the geometrical cross–section after the first interaction grows to a very large value:

$$\sigma_1 \sim \left(\frac{E_{\mathrm{str}}}{100 \mathrm{GeV}} \right) \times 10^4 \text{ mb} . \tag{5.12}$$

Inspired by such a large cross–section, one may ask how many interactions occur within the first–struck nucleus. Naively, the answer appears to be extremely large. The number of interactions is given by counting mfp's as the monopole travels through the nucleus:

$$N_{\mathrm{int}} \sim \int_0^{A^{1/3} \text{ fm}} dz \left[\lambda^{-1} = n_N \, \sigma \right] , \tag{5.13}$$

where here the appropriate nucleon density is that in a nucleus, $n_N \sim \mathrm{fm}^{-3}$. Note that N_{int} is a Lorentz invariant, as z and λ each scale the same way under a boost. For the cross-section above, one gets $N_{\mathrm{int}} \sim E_{\mathrm{str}}/\Lambda$. However, only that part of the string within the geometric cross section of the nucleus interacts. Furthermore, there is a causal limit on the rate at which the chromomagnetic string expands, and therefore on the rate at which the monopole cross-section grows. For a relativistic monopole, one expects the struck string to expand at nearly the speed of light. This leads

22

to a much more sober estimate for the number of interactions per first-struck nucleus, $N_{\text{int}} \sim A$. The number of interactions per subsequent struck nucleus is similar, as the cross-section saturates at the nuclear size $A^{2/3} \text{fm}^2$. On the other hand, the number of struck nuclei quickly becomes enormous. With the monopole traveling at near light speed, and the geometric cross-section growing also at near c, essentially all of the nuclei in the forward light–cone starting at the site of first interaction are struck, until the baryonic–monopole is quickly brought to rest.

In passing, we note an alternative possibility for a growing strong cross–section might be to enhance $(q$–monopole)–nucleon hard scattering relative to string–nucleon scattering, so that q–monopole recoil in the first interaction provides a large stretch to the string. The recoil energy can be significant, up to $\gamma m_N/2$, providing a stretch $\delta L \sim \gamma \Lambda^{-1}$, when the condition $M^2 \overset{<}{\sim} 2E_M m_N \sim (\text{PeV})^2$ holds. A schematic of q–monopole recoil is shown in figure (5d). The simplest way to increase the $(q$–monopole)–hadron cross–section is to increase the color-magnetic charge of one or more q–monopole constituents of the baryonic monopole. Increasing one constituent charge by an order of magnitude increases the cross-section by two orders of magnitude. Generally, the values of the constituent charges are model-dependent, with larger values typically coming from less attractive models. An added complication with a large $(q$–monopole)–nucleon cross–section is that the energy losses of baryonic–monopoles propagating through cosmic media and through the magnetic fields of the earth, sun, galaxy, etc. may require a re-analysis.

The baryonic–monopole's mfp $(\sigma_0 \rho_N)^{-1}$ for the first hadronic interaction is an observable and therefore of interest. We may estimate the unstretched baryonic–monopole "size" σ_0 by equating the energy stored in the string with that due to the repulsive magnetic force between the q–monopoles. This gives

$$\mu L_0 \simeq \frac{g^2}{L_0} \; . \tag{5.14}$$

Thus, the unstretched monopole's string length is

$$L_0 \sim \frac{g}{\sqrt{\mu}} \simeq \frac{6}{\Lambda} \; , \text{ where } g = \sqrt{\frac{137}{4}} \simeq 6. \tag{5.15}$$

The lateral size of the string is Λ^{-1} so that the geometric cross section is

$$\sigma_0 \sim 6\Lambda^{-2} \sim 60 \text{ mb} \left(\frac{200\text{MeV}}{\Lambda} \right)^2 \; . \tag{5.16}$$

This is somewhat larger than our order of magnitude estimate Λ^{-2}, but comparable to the cross–section of a high energy proton. Accordingly, we expect $X_{\max}$ for the baryonic–monopole to be similar to that of a proton, or even a nucleus.

We remark on a possible signature discriminating the monopole from a proton. The large number $n_{\text{emit}} \sim M/E_{\text{str}}$ of soft individual nuclear interactions underlying the monopole–induced shower event, in contrast to one of a few hard interactions from a primary proton, may lead to a larger hadron to electromagnetic ratio in the shower; this in turn leads to a higher muon content.

Finally, we remind the reader that the results of this section are predicated on a very speculative model wherein the strong cross–section of the baryonic–monopole grows very rapidly after the first interaction, and the particle emission rate from excited strings grows even more rapidly. While these dynamics are plausible, Nature may reject them. Then baryonic–monopoles will look much like l–monopoles in their interactions with matter.

VI. SUMMARY AND CONCLUSIONS

The challenge to seek a cosmic magnetic monopole flux below the Parker limit has now been met technologically in various underground/ice experiments. Here we provide theoretical motivation for further efforts to increase the search sensitivity.

The Kibble mechanism predicts possibly observable fluxes for monopoles with masses in the intermediate range, $10^{8\pm3}$ GeV. Such monopoles will be naturally accelerated by cosmic magnetic fields to relativistic energies. The Universe is transparent to relativistic monopoles meaning that a cosmic monopole flux should arrive at earth unattenuated and enter terrestrial detectors.

The possible signatures by which a relativistic monopole flux may be identified are varied. The Dirac condition for the monopole electromagnetic charge is $\alpha_M = 1/4\alpha$. This large coupling makes promising a search for electromagnetic signatures including direct Cherenkov emission, and coherent radio–Cherenkov emission from the charged $e^- - e^+$ shower. The radio signal may be observable for monopoles in polar ice. Of interest is the possibility of "m–raying" the interior of the earth with the monopole flux if their mass is within the range $3 \rightarrow 10$ PeV.

The hadronic properties of monopoles are not well known. Monopoles with color (q-monopoles) and without color (l-monopoles) are expected to be produced in phase transitions which break the gauge symmetry to the Standard Model. Just as the monopole magnetic charge is dual to electric charge, the monopole chromomagnetic charge is dual to the familiar chromoelectric charge. The l-monopoles carry QCD fields in their unbroken core, and so have a soft strong–interaction of size $\sigma \sim \Lambda_{QCD}^{-2}$. The q-monopoles may have a more interesting strong–interaction. Presumably they are confined by chromomagnetic strings into color–singlet baryonic–monopoles, with initial cross-section $\sigma_0 \sim \Lambda_{QCD}^{-2}$. In the process of interacting, the strings may not break until stretched to length at least $L \sim M/\mu$, where $\mu \sim \Lambda_{QCD}^2$ is the string tension. Thus, this stretching (if it can take place) will lead to a much larger cross–section if the energy-loss mechanisms of the string are slow compared to the interaction time. We have speculated that this enhanced cross–section may be many times larger than the usual QCD cross–section, and if so it could very quickly transfers $\mathcal{O}(1)$ of the monopole energy to the shower. In this case baryonic–monopoles would be viable candidates for the observed cosmic rays above $E_{GZK} \sim 5 \times 10^{19}$ eV.

VII. APPENDIX: SHOWER DEVELOPMENT MODEL

A monopole is highly penetrating and, as such, can initiate many subshowers before stopping. However, for a subshower to develop, the energy injected into the absorber in any single interaction must be greater than E_c. Thus, the inelasticity restriction $\eta \stackrel{>}{\sim} \frac{E_c}{E_0} \simeq 10^{-12} \left(\frac{E_0}{10^{20}\,\mathrm{eV}}\right)^{-1}$ holds for monopole-matter interactions which initiate subshowers, with lower inelasticity events contributing only to ionization.
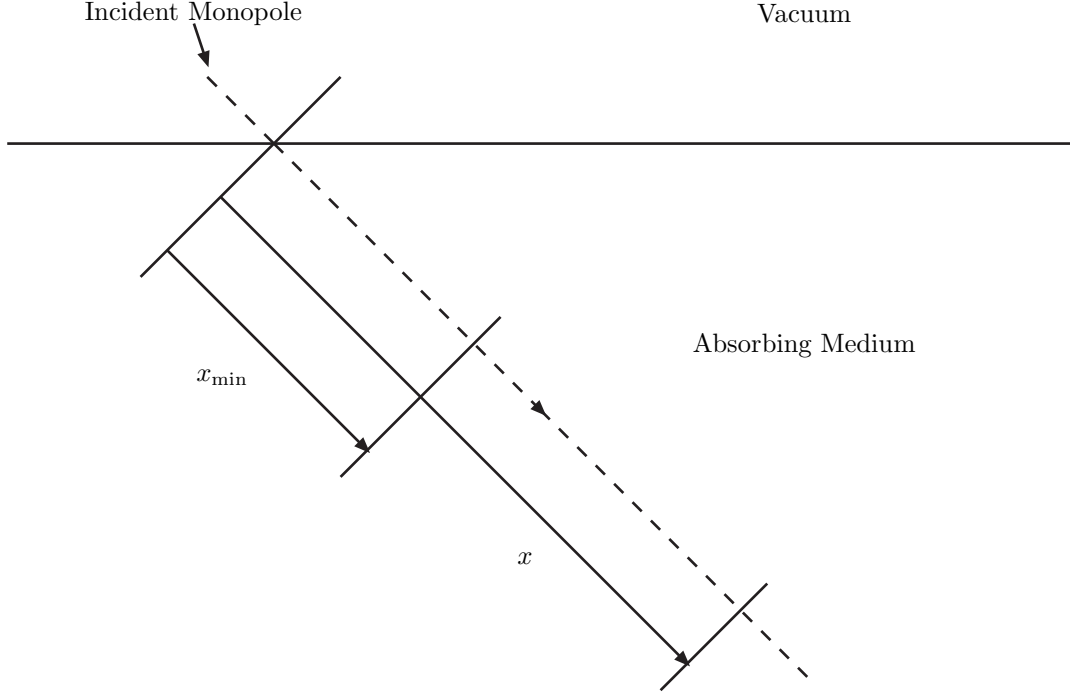
FIG. 6. A schematic representation of the variables entering into a calculation of the shower development for a monopole-induced shower. The monopole path is along the dashed line. The depth where the shower size is evaluated is at x. The smallest depth where an initiated subshower contributes to the total shower is $x_{\min}$.

Suppose the monopole initiates the jth subshower at a depth x_j. The subsequent development of the jth-subshower has particle number

$$N_j(x) = N_0 \, e^{\frac{(x - x_j)}{\xi_e}} \tag{7.1}$$

where $0 < (x - x_j) < \xi_e \ln\left(\frac{E_j}{N_0 E_c}\right)$, the total energy injected into the shower at the point x_j is E_j, and N_0 is the initial number of particles injected into the shower at the point x_j (For electron pair production $N_0 = 2$, whereas for bremsstrahlung and monopole-electron elastic scattering $N_0 = 1$.).

The total shower development $N(x)$ is then obtained by summing over all the subshowers

$$N(x) = \sum_j N_j(x). \tag{7.2}$$

The approximate distance between the initiation of subshowers is given by the monopole mean free path, $\lambda = \frac{1}{\sigma n}$, where σ is the monopole cross-section and n is the number density of scattering centers. The jth interaction then will roughly occur at the depth $x_j = j\lambda$. If the inelasticity per interaction is approximately given by a constant value of η then the energy injected at the jth scattering is

$$E_j = \frac{\eta}{1 - \eta}(1 - \eta)^j E_0. \tag{7.3}$$

The monopole will continue to initiate subshowers until [77] it is degraded in energy to the point where $E_j \simeq N_0 E_c$. That fixes the maximum number of subshowers to be

$$j_{\max} = \frac{\ln\left(\frac{(1-\eta)N_0 E_c}{\eta E_0}\right)}{\ln(1-\eta)}. \tag{7.4}$$

Note that this relation is just a restatement of the condition $0 < (x - x_j) < \xi_e \ln\left(\frac{E_j}{N_0 E_c}\right)$. The sum in eq. (7.2) can now be performed from $j = 1$ to $j = j_{\max}$.

The sum in eq. (7.2) can be transformed into an integral over column depth by making a continuum approximation. The substitutions $\sum_j \to \int \frac{dx_j}{\lambda}$ and $x_j \to x'$ give

$$N(x) = N_0 \int_{x_{\min}}^{x} \frac{dx'}{\lambda} e^{\frac{(x-x')}{\xi_e}} = N_0 \frac{\xi_e}{\lambda} \left[e^{\frac{(x-x_{\min})}{\xi_e}} - 1 \right]. \tag{7.5}$$

The physical interpretation of the limits of integration is as follows: $x_{\min}$ is the smallest depth at which an initiated subshower is still cascading at the depth x. Subshowers initiated at depths $< x_{\min}$ will have already ranged out by the point x [76], and so they cannot contribute to the particle number at x and are excluded from the integral.

From the geometry of fig. (6), using eqs. (4.3) and (7.3) and taking $j \to \frac{x}{\lambda}$, we can deduce

$$x_{\min}(x) = x - X_{\max}^j = x - \xi_e \ln\left(\frac{\eta(1-\eta)^{\frac{x_{\min}}{\lambda}} E_0}{(1-\eta)N_0 E_c}\right). \tag{7.6}$$

Solving for $x_{\min}$ gives

$$x_{\min} = \frac{x - \xi_e \ln\left(\frac{\eta E_0}{(1-\eta)N_0 E_c}\right)}{1 + \frac{\xi_e}{\lambda}\ln(1-\eta)}. \tag{7.7}$$

Using $\eta \ll 1$, so $\ln(1-\eta) \simeq -\eta$ and $\frac{\eta}{1-\eta} \simeq \eta$, this result simplifies to

$$x_{\min} = \frac{x - X}{1 - \frac{\eta \xi_e}{\lambda}}. \tag{7.8}$$

Here and in the remainder of this section we define $X \equiv X_{\max}^0 = \xi_e \ln\left(\frac{\eta E_0}{N_0 E_c}\right)$, which is the depth of the first subshower maximum (coming from a monopole with its full kinetic energy E_0). Expression (7.8) is formally singular at $\eta = \lambda/\xi_e \ll 1$, but for monopoles this singular point is not relevant.

For a monopole passing through matter, $\frac{\eta \xi_e}{\lambda} \ll 1$, so we can write eq. (7.8) as

$$x - x_{\min} = X - \frac{\eta \xi_e}{\lambda} x. \tag{7.9}$$

Substituting the above into eq. (7.5) gives the quasi steady–state shower size

$$N(x) \simeq \frac{\xi_e}{\lambda} \exp\left(\frac{X}{\xi_e}\right) \tag{7.10}$$

Notice that the x–dependence has vanished, as is appropriate for a steady–state phenomenon. Using the definition of X above, and the useful relation between the continuum and discrete expressions for energy loss

$$\frac{\eta E}{\lambda} = \left|\frac{dE}{dx}\right|, \tag{7.11}$$

we rewrite (7.10) as

$$N(\gamma) = \frac{\xi_e}{E_c} \left|\frac{dE_{\mathrm{pair}}}{dx}\right|_{\eta_{\mathrm{crit}} < \eta}, \tag{7.12}$$

26

where $\eta_{\text{crit}} \equiv \frac{200\text{MeV}}{E}$.
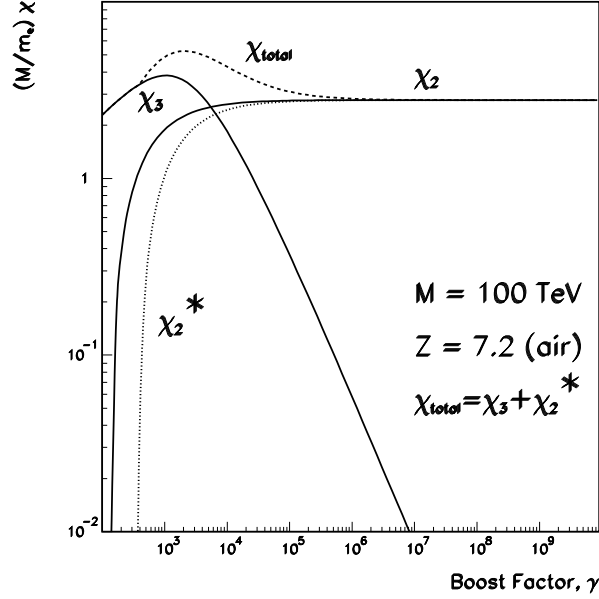

FIG. 7. Electron-positron pair production of an $M = 100$ TeV relativistic monopole in air where the inelasticity is restricted to $\eta > \eta_{\text{crit}} \equiv \frac{200\text{MeV}}{\gamma M}$.

We next turn to some details of the shower energy. In fig. (7) we plot the dominant terms for energy loss to electron–pair production, χ_2 and χ_3. For $\gamma \gtrsim 10^4$, pair production is dominated by χ_2, which describes slow pairs in the no screening limit. For shower development we must restrict the inelasticity to $\eta > \eta_{\text{crit}} \equiv \frac{200\text{MeV}}{E}$. The plot χ_2^* shows the effect of this restriction. Notice that $\chi_2^* \simeq \chi_2$ for $\gamma \gtrsim 10^5$, so we are justified in using eq. (3.8) without the η restriction to compute the shower size when $\gamma \gtrsim 10^5$. In the evaluation of eq. (7.12) we use a parameterization of ξ_e in different media (good to $\lesssim 2.5\%$) given by [78]

$$\xi_e = \frac{716.4\ A}{Z(Z+1)\ \ln\left(\frac{287}{\sqrt{Z}}\right)}\ \text{cm}^{-2} \tag{7.13}$$

and a fit to the data [79] for E_c :

$$\frac{E_c}{\text{MeV}} = \left\{ \begin{array}{ll} \frac{610}{Z+1.24} & \text{for solids and liquids} \\ \frac{710}{Z+0.92} & \text{for gases} \end{array} \right\}. \tag{7.14}$$

The contribution of the photonuclear process to the *electromagnetic* shower is indirect. The photonuclear interaction injects hadrons into the monopole shower. A subshower initiated by a high energy hadron will produce π^0's as secondaries, which each decay to 2 γ's. If these γ's have $E > E_c$, they may initiate an electromagnetic shower. So, only the largest inelasticity fraction of the energy lost via the photonuclear interaction contributes to the electromagnetic shower in the end. Given this fact, it is reasonable to assume that pair production alone provides a lower bound to the electromagnetic shower size and that the pair production plus photonuclear interaction provides an upper bound.
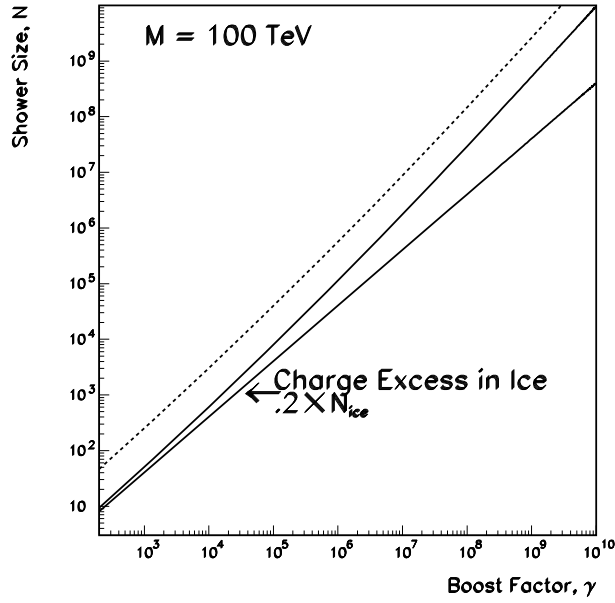
27

FIG. 8. The monopole-induced shower in ice for a monopole of mass 100 TeV. The shower size is the total number of electron, positrons, and photons. The dashed line is the total shower from pair production and the photonuclear interaction. The solid lines show the electric charge excess (roughly 20% of the shower size) for pair production alone ($\propto \gamma$) and pair production plus photonuclear ($\propto \gamma^{1.28}$).

3. Lateral Shower Profile

For monopole-induced showers the lateral profile is greatly simplified in comparison to hadronic primaries. As shown previously the monopole-induced shower is approximately constant, being continuously regenerated by the monopole as the lower energy particles range out. For our purposes in the following section it is sufficient to assume that the lateral profile is uniform out to a lateral cutoff given by the Molière radius

$$R_{\mathrm{M}} = 7.4\,\frac{\mathrm{g}}{\mathrm{cm}^2}\,\Big(\frac{\xi_e}{35\mathrm{g/cm}^2}\Big)\Big(\frac{100\mathrm{MeV}}{E_c}\Big). \tag{7.15}$$

As defined, the Molière radius is independent of the incident monopole energy, being determined only by the spread of low energy particles resulting from multiple Coulomb scattering. Within a distance R_{M} of the monopole path, ~ 90 % of the shower particles will be found [78].

ACKNOWLEDGEMENTS

[1] T. W. Kibble, Phys. Rept. **67**, 183 (1980), and references therein.

[2] Late–term phase transitions may temporarily break $U_{EM}(1)$, facilitating monopole annihilation. However, these models are rather contrived. See P. Langacker and S.–Y. Pi, Phys. Rev. Lett. **45,** 1 (1980); T.H. Farris, T.W. Kephart, T.J. Weiler, and T.C. Yuan, Phys. Rev. Lett. **68,** 564 (1992); V.V. Dixit and M. Sher, Phys. Rev. Lett. **68,** 560 (1992).

[3] G. Giacomelli, et al., Magnetic Monopole Bibliography, DFUB 9/98 (1998).

[4] E. N. Parker, Astrophys. J. **160**, 383 (1970); *ibid.* , **163**, 225 (1971); *ibid.* ,**166**, 295 (1971). Based on more speculative hypotheses, more stringent bounds have been proposed for the galactic flux by M.S. Turner, E.N. Parker, and T. J. Bogdan, Phys. Rev. **D26**, 1296 (1982); and for the extragalactic flux by Y. Rephaeli and M. S. Turner, Phys. Lett. **121B**, 115 (1983); F. Adams et al., Phys. Rev. Lett. **70**, 2511 (1993); M.J. Lewis, K. Freese, and G. Tarle, [astro-ph/9911095]. It is not clear to us that any of these bounds apply to a relativistic flux of monopoles; a relativistic monopole traveling through a plasma may actually create magnetic fields in its wake.

[5] N.A. Porter, Nuovo Cim. **16**, 958 (1960); E. Goto, Prog. Theo. Phys. **30**, 700 (1963).

[6] T.W. Kephart and T.J. Weiler, Astropart. Phys. **4** 271 (1996); Nucl. Phys. (Proc. Suppl.) **51B**, 218 (1996).

[7] G. 't Hooft, Nucl. Phys. **B79,** 276 (1974); A. Polyakov, JETP Lett. **20,** 194 (1974).

[8] For a review and references see: M. B. Hindmarsh and T. W. Kibble, Rept. Prog. Phys. **58**, 477 (1995) [hep-ph/9411342].

[9] A. De Rujula, Nucl. Phys. **B435**, 257 (1995).

[10] Due to the smallness of the monopole's Thomson cross–section for monopole masses of interest, $\sigma_T \sim 2 \times 10^{-43}(10^{10}\text{GeV}/M)^2\text{cm}^2$, the mean free path for a monopole to scatter on the cosmic background radiation greatly exceeds the Hubble size of the Universe [6].

[11] S. F. King and Q. Shafi, Phys. Lett. **B422**, 135 (1998) [hep-ph/9711288].

[12] D.K. Hong, J. Kim, J.E. Kim, and K.S. Soh, Phys. Rev. **D27**, 1651 (1983).

[13] N. G. Deshpande, B. Dutta and E. Keith, Nucl. Phys. Proc. Suppl. **52A**, 172 (1997) [hep-ph/9607307]; Phys. Lett. **B388**, 605 (1996) [hep-ph/9605386]; Phys. Lett. **B384**, 116 (1996) [hep-ph/9604236].

[14] P. H. Frampton and B. Lee, Phys. Rev. Lett. **64**, 619 (1990); P. H. Frampton and T. W. Kephart, Phys. Rev. **D42**, 3892 (1990).

[15] M. Maldacena, Adv. Theor. Math. Phys. **D42**, 231 (1998).

[16] P. H. Frampton, Phys. Rev. **D60**, 121901 (1999) [hep-th/9907051].

[17] P. H. Frampton, Phys. Rev. **D60**, 085004 (1999) [hep-th/9905042]; P. H. Frampton and T. W. Kephart, [hep-th/9912028].

[18] K. R. Dienes, E. Dudas, and T. Gherghetta, Phys. Lett. **B436**, 55 (1998) [hep-ph/9803466].

[19] I.Antoniadis, N. Arkani-Hamed, S. Dimopoulos, and G. Dvali, Phys. Lett. **B436**, 257 (1998). [hep-ph/9804398]

[20] C.L. Gardner and J.A. Harvey, Phys. Rev. Lett. **52,** 879 (1984).

[21] T. Vachaspati, Phys. Rev. Lett. **76**, 188 (1996) [hep-ph/9509271]; H. Liu and T. Vachaspati, Phys. Rev. **D56**, 1300 (1997) [hep-th/9604138].

[22] A. S. Goldhaber, Phys. Rept. **315**, 83 (1999) [hep-th/9905208].

[23] For a review see P. P. Kronberg, Rept. Prog. Phys. **57**, 325 (1994); galactic cluster fields are updated in T.E. Clark, P.P. Kronberg, and H. Boehringer, to appear in Ap. J. Lett., [astro-ph/0011281].

[24] E. Huguet and P. Peter, Astropart. Phys. **12**, 277 (2000) [hep-ph/9901370].

[25] D. Ryu, H. Kang, and P.L. Biermann, Astron. & Astrophys. **335**, 19 (1998) [astro-ph/9803275].

[26] K.-T. Kim et al., Nature **341**, 720 (1989).

[27] R. Beck, Ann. Rev. Astron. & Astrophys. **34**, 155 (1996).

[28] P.P. Kronberg, P.L. Biermann and F.R. Schwab, Astrophys. J. **291**, 693 (1985).

[29] K.I. Kellermann and I.I.K Pauliny-Toth, Ann. Rev. A&A **19**, 373 (1981).

[30] T.A. Enßlin, et al., Astrophys. J. **477**, 560 - 567 (1997).

[31] R. Plaga, *Nature* **374**, 430 (1995).

[32] A third possible type of GUT monopoles is truly "color blind." For example, an E_6 GUT with breaking scheme $E_6 \rightarrow SU_C(3) \times SU_L(3) \times SU_R(3) \rightarrow SU_C(3) \times SU_L(2) \times U_Y(1)$ has monopoles with no hadronic interaction whatsoever.

[33] In cgs units, $\alpha = e^2/4\pi$, $\alpha_M = g^2/4\pi$, and $g\,e = 2\pi$. In Heaviside-Lorentz units, $\alpha = e^2$, $\alpha_M = g^2$, and $g\,e = \frac{1}{2}$. In either set of units, $g = e/2\alpha$ and $\alpha_M = 1/4\alpha$.

[34] Recent progress in quantizing the interacting monopole can be found in M. Blagojevic and P. Senjanovic, Phys. Rept. **157**, 233 (1988); L. Gamberg and K. A. Milton, hep-ph/9910526.

[35] G. Giacomelli, in: *Theory and Detection of Magnetic Monopoles in Gauge Theories,* ed. N. Craigie p.407 (Singapore: World Scientific Publishing Co., 1986).

[36] S.P. Ahlen, Rev. Mod. Phys. **52,** 121 (1980).

[37] L.D. Landau and E.M. Lifshitz, *Electrodynamics of Continuous Media,* (Oxford: Pergamon Press, 1984).

[38] L.D. Landau and E.M. Lifshitz, *Relativistic Quantum Mechanics,* (Oxford: Pergamon Press, 1984).

[39] R.M. Sternheimer, R.F. Peierls, Phys. Rev. B **3,** 3681 (1971).

[40] S.R. Kel'ner and Yu.D. Kotov, Sov. Jour. Nucl. Phys. **7,** 237 (1968); S.R. Kel'ner, Sov. Jour. Nucl. Phys. **5,** 778 (1967).

[41] J. D. Jackson, *Classical Electrodynamics*, (New York: John Wiley and Sons, 1975).

[42] For bremsstrahlung, screening of the nuclear charge by the atomic electrons is large when [41]

$$\gamma > \frac{192M}{m_e Z^{\frac{1}{3}}} \simeq \frac{3 \times 10^{10}}{Z^{\frac{1}{3}}} \left(\frac{M}{100 \text{TeV}} \right) . \tag{7.16}$$

Even for the lightest monopoles which we consider (40 TeV), eq. (7.16) shows that screening corrections are expected to be small.

[43] S.I. Dutta, M.H. Reno, I. Sarcevic, and D. Seckel, Phys. Rev. D **63,** 094020 (2001) [hep-ph/0012350].

[44] W. Heitler, *The Quantum Theory of Radiation,* (Oxford: Clarendon Press, 1954).

[45] T.K. Gaisser, *Cosmic Rays and Particle Physics,* (Cambridge: Cambridge University Press, 1990); or A. M. Hillas, *Ann. Rev. Astron. Astrophys.* **22**, 425 (1984).

[46] P. Sokolsky, *Introduction to Ultrahigh Energy Cosmic Ray Physics*, (New York: Addison-Wesley Publishing Company, 1989).

[47] The particle doubling length R can be lengthened significantly by the Landau-Pomeranchuk-Migdal effect [48,49] for photon or electron energies $E \stackrel{>}{\sim} E_{\text{LPM}}$. The value of E_{LPM} is dependent on the material and some typical values are $E_{\text{LPM}} = 2.2$ TeV for lead, $E_{\text{LPM}} = 139$ TeV for water, and $E_{\text{LPM}} = 117$ PeV for sea level air [48]. This model assumes that $E \ll E_{\text{LPM}}$ which is generally the case for $e^{\pm}$ and γ originating from monopole–nucleus interactions.

[48] S. Klein, [astro-ph/9712198]; ibid, Rev. Mod. Phys. **71,** 1501 (1999).

[49] L.D. Landau and I.J. Pomeranchuk, in *The Collected Papers of L.D. Landau,* (Oxford: Pergamon Press, 1965); A.B. Migdal, Phys. Rev. **103,** 1811 (1956).

[50] E. Zas, F. Halzen, and T. Stanev, Phys. Rev. D **45,** 362 (1992).

[51] R. Clay and P. Gerhardy, Australian J. Phys. **35,** 59 (1982).

[52] E. Fermi, Phys. Rev. **57,** 485 (1940).

[53] R. Hagstrom, *Phys. Rev. Lett.* **35**, 1677 (1975).

[54] V.A. Balkanov et al. (Baikal Collaboration), 26th International Cosmic Ray Conf. (ICRC99), Salt Lake City, UT, Aug. 17-25, 1999, paper H.E.5.3.04.

[55] P. Niessen et al. (AMANDA Collaboration), 26th International Cosmic Ray Conf. (ICRC99), Salt Lake City, UT, Aug. 17-25, 1999, paper H.E.5.3.05.

[56] B.C. Choudhary et al. (MACRO Collaboration), 26th International Cosmic Ray Conf. (ICRC99), Salt Lake City, UT, Aug. 17-25, 1999, paper H.E.5.3.02.

[57] F. Halzen, private communication.

[58] The charge excess results from a number of processes involving the shower interacting with the medium. These include knock-on electrons, Compton scattering, and positron annihilation.

[59] G.A. Askar'yan, Sov. Phys. JETP **14**, 441 (1962); *ibid.*, **48**, 988 (1965); M.A. Markov and I.M. Zeleznykh, Nucl. Instrum. Methods A **248**, 242 (1986).

[60] G.M. Frichter, J.P. Ralston, and D.W. McKay, Phys. Rev. D **53,** 1684 (1996).

[61] Calculations of the energy loss of monopoles and dyons passing through the Earth and in scintillators, streamer tubes, nuclear track detectors is given in J. Derkaoui, Astro. Part. Phys., **9,** 173 (1998); Astro. Part. Phys., **10,** 339 (1999).

[62] For example, the energy threshold for Fly's Eye is $\sim 10^{17.3}$ eV [63] which renders the Eye blind to l-monopoles, except for those with the smallest allowed mass at the greatest allowed kinetic energies.

[63] D. J. Bird et al. (Fly's Eye Collab.), Astrophys. J. **424**, 491 (1994); *ibid.* **441**, 144 (1995).

[64] T. Lay and T.C. Wallace, *Modern Global Seismology*, (New York: Academic Press, 1995).

[65] Properties of the Solid Earth, in Rev. Geophys. **33,** (1995); also at the URL: http://earth.agu.org/revgeophys.

[66] This idea has been exploited in neutrino physics as neutrinos are sufficiently weakly interacting to pass through the earth largely unimpeded for neutrino energies $\lesssim 10^{15}$ eV.

[67] A.M. Dziewonski and D.L. Anderson, Phys. Earth Planet. Inter. **25,** 297 (1981).

[68] In principle, the eight shell model could be used in our calculations but it provides more detail than is needed here. The two shell approximation includes the gross features necessary to show tomography with monopoles.

[69] K.B. Krauskopf and D.K. Bird, *Introduction to Geochemistry* (New York: McGraw-Hill Publishers, 1995).

[70] The angular resolution of earth tomography with monopoles is, in principle, limited by the multiple scattering of the monopole through small angles. However, the large monopole mass renders this angular uncertainty negligibly small.

[71] T.J. Weiler, hep-ph/9910316, based on private communication from A.A. Watson.

[72] R.N. Mohapatra and S. Nussinov, Phys. Rev. **D57**, 1940 (1998); in I.F.M. Albuquerque, G. Farrar, and E.W. Kolb, Phys. Rev. **D59**, 015021 (1999) it is noted that a baryon mass above 10 GeV produces a noticeably different shower profile, and a baryon mass above 50 GeV is so different as to be ruled out.

[73] In the other extreme, it has been proposed [74] that the origin of the superGZK events are the gauge bosons radiated by cosmic monopole–string networks when the stretched strings relax.

[74] V. Berezinsky, X. Martin, and A. Vilenkin, Phys. Rev. **D56**, 2024 (1997); V. Berezinsky and A. Vilenkin, Phys. Rev. Lett. **79**, 5202 (1997); V. Berezinsky, P. Blasi, and A. Vilenkin [astro-ph/9803271].

[75] More exactly, $\sum_{n=1}^{N} = \ln N + \gamma_E + \frac{1}{2N} + \mathcal{O}(\frac{1}{N^2})$, where $\gamma_E = 0.577\ldots$ is Euler's constant; this formula can be found on p. 2 of I.S. Gradshteyn and I.M. Ryzhik, *Tables of Integrals, Series, and Products*, (New York: Academic Press 1980).

[76] We neglect particles after their energies fall below E_c. Omission of this exponentially–decaying tail results in an underestimate of the true particle number by a factor of order a few. This makes a small difference as far as the coherent–shower

Cherenkov emission is concerned. It makes more difference to the longitudinal profile, and therefore to the fluorescence signal. However, we show in section (IV C) that the fluorescence signal from a monopole is weak, probably too weak to be measured.

[77] Our cutoff on shower development for particles with energy below $E_c = 200$ MeV is conservative. For example, an e^+e^- pair produced by a 50 MeV photon yields 25 cm of tracklength in ice, along which the pair will generate Cherenkov light, delta rays, and further ionization.

[78] Particle Data Group, Phys. Rev. D **50**, 1173 (1994).

[79] B. Rossi, *High-Energy Particles*, (New York: Prentice-Hall, 1952).